

**FLUIDIZED-BED OXIDATIVE DEHYDROGENATION
OF n-BUTANE TO BUTENE OVER VO_x/Ce-Al₂O₃:
CATALYST DEVELOPMENT AND REACTION
KINETICS**

BY

MUHAMMAD YASIR KHAN

A Thesis Presented to the
DEANSHIP OF GRADUATE STUDIES

KING FAHD UNIVERSITY OF PETROLEUM & MINERALS

DHAHRAN, SAUDI ARABIA

In Partial Fulfillment of the
Requirements for the Degree of

MASTER OF SCIENCE

In

CHEMICAL ENGINEERING

NOVEMBER 2015

KING FAHD UNIVERSITY OF PETROLEUM & MINERALS

DHAHRAN- 31261, SAUDI ARABIA

DEANSHIP OF GRADUATE STUDIES

This thesis, written by **MUHAMMAD YASIR KHAN** under the direction of his thesis advisor and approved by his thesis committee, has been presented and accepted by the Dean of Graduate Studies, in partial fulfillment of the requirements for the degree of **MASTER OF SCIENCE IN CHEMICAL ENGINEERING**.



Dr. **Mohammad M. Hossain**
(Advisor)



Dr. **Mohammad S. Ba-Shammakh**
Department Chairman

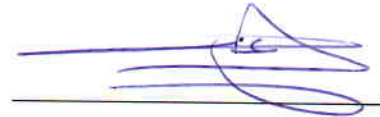


Dr. **Shaikh A. Razzak**
(Co-Advisor)



Dr. **Salam A. Zummo**
Dean of Graduate Studies





Dr. **Abdalla A. Al-Shammari**
(Member)

22/12/15
Date



Dr. **Mohammad S. Ba-Shammakh**
(Member)



Dr. **Sameer Al-Ghamdi**
(Member)

© Muhammad Yasir Khan

2015

Dedicated

To my parents, to my teachers
and to my brother Muhammad Nasir Khan |

ACKNOWLEDGMENT

In the name of ALLAH, The Most Merciful and The Most Gracious

I would like to express my appreciation and sincere thanks to my advisor Dr. Mohammad Mohazar Hossain for his support, inspiration and guidance throughout my thesis work. Throughout my experimental period, he provided encouragement, good teaching and lot of good ideas. My gratitude goes to my thesis co-advisor Dr. Shaikh Abdur Razzak for his continuous support, technical knowledge and supervision.

I am also very grateful to my Thesis Committee Members; Dr. Sameer Al-Ghamdi, Dr. Abdallah A. Al-Shammari and Dr. Mohammad S. Ba-Shammakh for their precious comments, valuable suggestions and technical support.

I would like to acknowledge King Fahd University of Petroleum and Minerals for giving me an opportunity to pursue MS degree at Chemical engineering department and I would also appreciate King Abdul Aziz City for Science and Technology (KACST) for funding my MS project under research grant #. APR-30-252. My heartfelt thanks to all faculty members of chemical engineering department, especially Dr. Nayef Masnad Al-Saifi and Dr. Housam Binous.

An acknowledgment would not be complete without appreciating my parents, my brothers and my sweet sisters, for their continuous prayers and encouragements. Finally, I would like to thanks our catalysis group members especially, Abdul Hafeez Ayandiran and the lab technicians: Syed Amanullah, and Mariano Tarle Gica. My special appreciations goes to Farrukh Shehzad, Syed Abdul Salam, Muhammad Irfan Malik, Murad Ali, Mohammad Daud Jan, Ihsanullah, and Kashif Rehan.

|

TABLE OF CONTENTS

ACKNOWLEDGMENT	V
TABLE OF CONTENTS.....	VI
LIST OF TABLES.....	IX
LIST OF FIGURES.....	X
LIST OF ABBREVIATIONS.....	XIII
LIST OF SYMBOLS	XIV
ABSTRACT.....	XV
ملخص الرسالة	XVI
CHAPTER 1 INTRODUCTION.....	1
1.1 Background	1
1.2 Conventional routes for C4-Olefins production	4
1.3 Oxidative Dehydrogenation (ODH).....	7
1.3.1 Motivation for using Novel ODH.....	11
CHAPTER 2 LITERATURE REVIEW	14
2.1 Type of the catalyst system used for the ODH of Butane	15
2.2 Unsupported catalysts	16
2.3 Supported catalysts	17
2.4 Promoters.....	19
2.5 Kinetic Modeling	19
2.6 Motivations	21

2.7	Conclusion of Literature Review.....	22
CHAPTER 3 OBJECTIVES		25
3.1	Main Objectives	25
3.2	Specific Objectives	25
CHAPTER 4 EXPERIMENTAL PROCEDURE.....		27
4.1	CATALYST SYNTHESIS	27
4.1.1	Catalyst Preparation.....	27
4.1.2	Chemical used	27
4.1.3	Support preparation.....	28
4.1.4	Synthesis of Ceria/MAs	28
4.1.5	Active site preparation	29
4.2	Catalyst Characterization	30
4.2.1	Field emission scanning electron microscopy (FE-SEM)	31
4.2.2	X-ray diffraction (XRD) analysis	32
4.2.3	Raman Spectroscopy	32
4.2.4	Fourier transform infrared spectroscopy (FTIR)	33
4.2.5	Thermogravimetric analysis	33
4.2.6	Temperature programmed desorption (TPD)	33
4.2.7	Temperature programmed reduction and oxidation (TPR/TPO)	35
4.3	ODH in the CREC Riser Simulator.....	36
CHAPTER 5 RESULTS AND DISCUSSION.....		40
5.1	Catalyst Characterization Results	40
5.1.1	FE-SEM analysis	40
5.1.2	X-ray diffraction (XRD) analysis results	43

5.1.3	Raman spectroscopy	45
5.1.4	FTIR spectroscopy.....	47
5.1.5	Thermogravimetric analysis	48
5.1.6	Total acidity and metal support interaction (NH ₃ -TPD).....	49
5.1.7	Temperature programmed reduction (TPR).....	56
CHAPTER 6 ODH OF N-BUTANE AND REACTION KINETICS		63
6.1	Catalyst Evaluation in Fluidized bed reactor.....	63
6.2	Kinetic Model formulation	75
6.3	Kinetic parameter estimation	78
6.4	Comparison with the literature	82
CHAPTER 7 CONCLUSIONS AND RECOMMENDATIONS		83
7.1	Conclusions.....	83
7.2	Recommendations	84
REFERENCES.....		85
VITAE.....		98

LIST OF TABLES

Table 2.1. Summary of the literature review	24
Table 4.1. Synthesized catalysts and their nomenclature	30
Table 5.1. Total acidity and maximum reduction temperature	51
Table 5.2. Estimated Desorption parameters at $\beta = 10 \text{ }^\circ\text{C}/\text{min}$	55
Table 6.1. Estimated kinetic parameters at $450 \text{ }^\circ\text{C}$	80

LIST OF FIGURES

Figure 1.1. Total Consumption of light olefins 205 M ton [7].	3
Figure 1.2. Recorded and forecasted Light Olefin Consumption for the period 2004-2017 [7].....	3
Figure 1.3. Global volume of C4-olefins by process types [5].....	6
Figure 1.4. Schematic of Fixed-bed ODH in the presence of gas phase oxygen.....	8
Figure 1.5. Novel gas phase oxygen free ODH schematic.	9
Figure 1.6. Gas phase O ₂ free novel ODH.....	10
Figure 1.7. Drawbacks associated with the traditional routes for C4-olefins production [8].....	11
Figure 4.1. Process Schematic for NH ₃ -TPD characterization, Micromeritics AutoChem-II.....	34
Figure 4.2. CREC Riser Simulator reactor assembly	36
Figure 4.3. Schematic Diagram of the CREC Riser Simulator experimental set-up.....	38
Figure 5.1. Secondary Electron images (SEI) of the (a) MAs (b) 0.2 Ce (c) 1.0 Ce (d) 5.0 Ce	42
Figure 5.2. XRD spectra of (a) MAs (b) VO _x /γ-Al ₂ O ₃ (c) 0.2 Ce (d) 1.0 Ce (e) 3.0 Ce (f) 5.0 Ce	44
Figure 5.3. Raman spectra of the (a) MAs support, (b) 0.2 Ce, (c) 3.0 Ce, and (d) 5.0 Ce catalysts.....	46
Figure 5.4. FTIR spectra of (a) 0.2 Ce (b) 1.0 Ce (c) 3.0 Ce (d) 5.0 Ce.....	47
Figure 5.5. TGA Weight loss curves (a) 0.2 Ce (b) 1.0 Ce (c) 3.0 Ce (d) 5.0 Ce	48

Figure 5.6. NH ₃ -TPD analysis: TCD signal vs Temperature for 0.2 Ce, 1.0 Ce, 3.0 Ce and 5.0 Ce catalysts	50
Figure 5.7. TPR profile of (a) 0.2 Ce (b) 1.0 Ce (c) 3.0 Ce (d) 5.0 Ce	58
Figure 5.8. H ₂ consumption for 0.2 Ce, 1.0 Ce, 3.0 Ce, and 5.0 Ce catalysts	59
Figure 5.9. TPR/TPO cycles of 0.2 Ce catalyst	60
Figure 5.10. The % reduction of vanadium	62
Figure 6.1 Blank run (2 ml butane injection, t=10 sec)	65
Figure 6.2. The typical product distribution for the ODH of n-butane over the two extreme condition of the temperature (450 & 600 °C) on 0.2 Ce catalyst (t = 10 s, w = 1 g, feed = 1 ml)	67
Figure 6.3. Effect of butane conversion, C ₄ -olefins selectivity and CO _x selectivity on 0.2 Ce, 1.0 Ce, 3.0 Ce and 5.0 Ce catalysts, ● C ₄ -olefins selectivity, ■ CO _x selectivity, ▲ butane conversion (t = 10 s, w = 1 g, feed = 1 ml, T = 500 °C)	69
Figure 6.4. Effect of temperature on product selectivity, 0.2 Ce Catalyst (t = 10 , 15, 25 s, w = 1 g, feed = 1 ml)	70
Figure 6.5. Effect of contact time on C ₄ -olefins selectivity over 0.2 Ce catalyst, ● C ₄ -alkenes sele. at 450 °C, ▲ C ₄ -alkenes sele. at 550 °C, ■ n-butane conv. at 550 °C, ◆ n-butane conv. at 450 °C (feed = 1 ml, w = 1 g)	71
Figure 6.6. Butane conversion and C ₄ -olefins selectivity over 0.2 Ce catalyst in consecutive ODH runs with catalyst re-oxidation (T = 450 °C, t = 10 s, w = 1 g, feed = 1 ml)	72

Figure 6.7. Effect of successive injection, T=500°C, t=5sec, 0.2% Ceria doped cat, feed/cat=0.5	73
Figure 6.8. Parallel, series reaction network.....	76
Figure 6.9. Experimental data points and model prediction vs observation number.....	78
Figure 6.10. Model predicted (continuous line) mole fraction and experimental data points (circles) for both CO _x and for C4-olefins at 550°C	81
Figure 6.11. Model predicted (continuous line) mole fraction and experimental data points (circles) for both CO _x and for C4-olefins at 550°C	81

LIST OF ABBREVIATIONS

ODH	:	Oxidative dehydrogenation
C4-olefins	:	Sum of 1, cis, iso-butene and 1, 3-butadiene
MAs	:	Mesoporous alumina
XRD	:	X-ray diffractometry
TPD	:	Temperature programmed desorption
TPR	:	Temperature programmed reduction
TPO	:	Temperature programmed oxidation
Ce-MAs	:	Ceria modified mesoporous alumina
MO	:	Metal oxide

LIST OF SYMBOLS

wt	:	Weight percentage
T	:	Temperature
T_n	:	Centering temperature
R	:	Universal gas constant
M	:	Million
S	:	Selectivity
C	:	Conversion
V_m	:	Total volume of ammonia desorbed
E_{des}	:	Activation energy for desorption
k_i	:	Reaction rate constant
K_i	:	Adsorption constant

Greek letters

γ	:	Gemma
β	:	Temperature ramp
θ_i	:	Surface coverage

|

ABSTRACT

Full Name : [MUHAMMAD YASIR KHAN]

Thesis Title : FLUIDIZED-BED OXIDATIVE DEHYDROGENATION OF n-BUTANE TO BUTENE OVER VO_x/Ce-Al₂O₃: CATALYST DEVELOPMENT AND REACTION KINETICS

Major Field : [CHEMICAL ENGINEERING]

Date of Degree : [November 2015]

Mesoporous γ -Al₂O₃ (MAs) and Ceria doped MAs (Ce-MAs) supports were prepared with different wt% of ceria (0.2-5 wt%) by facile free synthesis method. VO_x was impregnated on these modified supports by excessive solvent impregnation method. The XRD, Raman, and FTIR characterization techniques indicated the presence of crystalline CeO₂, and amorphous VO_x phases on the MAs support. TPR/TPO analysis revealed that VO_x/Ce-MAs catalysts are not only very active but also very stable over the repeated reduction/oxidation cycles. NH₃-TPD characterization along with desorption kinetic results showed that the prepared catalysts had mild acidity. The low activation energy for desorption presented a weak metal-support interaction. Fluidized-bed, oxidative dehydrogenation (ODH) of n-butane experiments over VO_x/Ce-MAs catalysts were investigated under anaerobic condition in CREC Riser Simulator. Temperature and contact time was varied from 450-600 °C and 5-25 sec, respectively. The maximum selectivity (62.3%) of C₄-olefins was observed at 450 °C and 5 sec over the catalyst containing lowest ceria wt% (0.2 wt%). The successive butane injection without catalyst regeneration showed that the selectivity of the C₄-olefins is directly related with the degree of the catalyst reduction. Finally, experimental data was fitted into kinetic model based on Langmuir-Hinshelwood model that incorporates exponential catalyst decay term into the rate of reaction equation. Overall, the regression analysis has shown a good fitting for the estimation of kinetic parameters. At the low reaction temperature (450 °C) the kinetic model predicted low activation energy (130.1 kJ mol⁻¹) for the C₄-alkenes formation, as compared to high activation energies noticed for the undesired deep oxidation of the feed (135.1 kJ mol⁻¹) and C₄-olefins (149.9 kJ mol⁻¹).

ملخص الرسالة

الاسم الكامل: محمد ياسر خان

عنوان الرسالة: الأكسدة الإنتقائية بإنتزاع الهيدروجين من البيوتان, تحضير العامل الحفّاز والنمذجة الحركية

التخصص: هندسه كيميائيه

تاريخ الدرجة العلمية: تشرين الثاني 2015

أكسيد الألومنيوم المثقب وأكسيد الألومنيوم المشوب بأكسيد السيريوم تم تحضيرها بإضافة نسب وزنيه مختلفه من أكسيد السيريوم (من 0.2 إلى 5 % وزنياً) بإستخدام طريقه التحضير السطحي الحر. أكسيد الفانديوم تم تشريبه على هذه الدعائم المحوّره بإستخدام طريقة التشريب الزائد للمذيبات. تقنيات تحديد الخصائص مثل إنحراف الأشعه السينيه, وطيف رامان وطيف الأشعه تحت الحمراء دلّت على وجود أكسيد السيريوم المتبلور, وأكسيد الفناديوم غير المتبلور. تحليل الأكسده والإختزال لدرجة الحراره المبرمه كشفت أن دعائم أكسيد الألومنيوم على دعائم أكسيد الألومنيوم. المشوبه بأكسيد السيريوم المشربه بأكاسيد الفانديوم بالإضافه إلى نشاطها العالي فإنها تتميز بإستقرار عالي يتضح ذلك من تكرار دورات الأكسده والإختزال. درجة الحراره المبرمه لإمتزاز جزيئات الأمونيا مع نتائج الإمتزاز الحركيه أظهرت أن العوامل الحفّازه المحضره لها حمضيه خفيفه. طاقة التنشيط المنخفضه للإمتزاز تبين ضعف التداخل بين المعدن والدعائم. القواعد المميعة, تجارب نزع الهيدروجين التأكسديه من غاز البيوتان على دعائم أكسيد الألومنيوم المشوبه بأكسيد السيريوم المشربه بأكسيد الفانديوم تم إجراءها تحت ظروف لا هوائيه فى المحاكى الرافع المطور فى مركز مفاعل الهندسه الكيمائيه. درجة الحراره و زمن التلامس تم تغييرها من 450 إلى 575 درجة مؤويه و 5 إلى 25 ثانيه على التوالي. الإنتقائيه القصوى كانت 62.3 % للأوليفينات المحتويه على أربع ذرات كربون تم ملاحظتها عند درجة حراره 450 درجة مؤويه و 5 ثوانى زمن تلامس للعامل الحفاز المحتوى على أقل كميّه من أكسيد السيريوم (0.2%). الحقن المتتابع للبيوتان بدون تجديد الحفّاز للأوليفينات المحتويه على أربع ذرات كربون ترتبط مباشرةً مع درجة إختزال العامل الحفّاز. وأخيراً البيانات التجريبيه تم إخضاعها على نموذج حركى إستناداً على نموذج لانجمور- هينشيلود الذى يتضمن الإنحلال الأسى للعامل الحفاز فى معدل معادله التفاعل. بصوره عامه فقد أظهرت تحاليل الحركه التراجعيه توافقاً كبيراً لمعايير الحركيه التى تم تقديرها.

CHAPTER 1

INTRODUCTION

The use of commercially available and economical feedstock such as ethane, propane, and butane are very important for today's petrochemical industry to claim sustainable development [1]. This is due to the fact that the process industries' energy requirement mainly depends on the crude oil: which is running out and cannot last for another century. At the same time, the current renewable energy resources are in the developing stages; thus cannot completely replace the tradition energy resources. So, the effective utilization of globally available alkanes (C1-C4) in the form of natural gas, could become the major energy source, and building blocks for 21st century chemical industries. In fact, there is a huge economic incentive of converting these short chain paraffins to more valuable light olefins.

1.1 Background

The light alkenes, specially butene isomers and 1, 3-butadiene (C4-olefins) are the chemicals of relevance importance, as they are used in the production of gasoline additives, styrene-butadiene rubber (SBR), Nitrile-butadiene rubber (NBR), alkylate, maleic anhydride, polybutadiene, polyamides, and they also act as intermediate in the synthesis of various polymers and chemicals [2–4].

Conventionally, C4-olefins are produced by fluid catalytic cracking, steam cracking, and catalytic dehydrogenation [5]. For instance, there are two methods for the manufacturing of butadiene in the United States namely: 1) the indirect synthesis scheme, and 2) the direct synthesis method. The former method is used by the Philips process industry, and in that process the starting material is n-butane: which is converted to an intermediate butene and then in second step it's finally converted to butadiene. Houdry Catadiene process uses direct method for the conversion of n-butane to butadiene, in this method n-butene is also introduced with the feed [6].

Figure 1.1 shows the typical consumption areas for the light alkenes, as it can be seen that, they are mainly used for the production of polyethylene and polypropylene [7]. Figure 1.2 shows the time rate of increase in the consumption of olefins. A linear increase in the demand of the olefins for the coming years is expected, e.g., the current consumption rate of butadiene is ~ 0.24 billion tons in 2015, while the forecasted consumption rate will increase to 0.27 billion tons in 2017, that in turn will create large gap between the production and consumption of C4-olefins [7]. It is evident from the Figure 1.2, that the C4-olefins has the highest supply and consumption difference as compared with the other short chain unsaturated hydrocarbons.

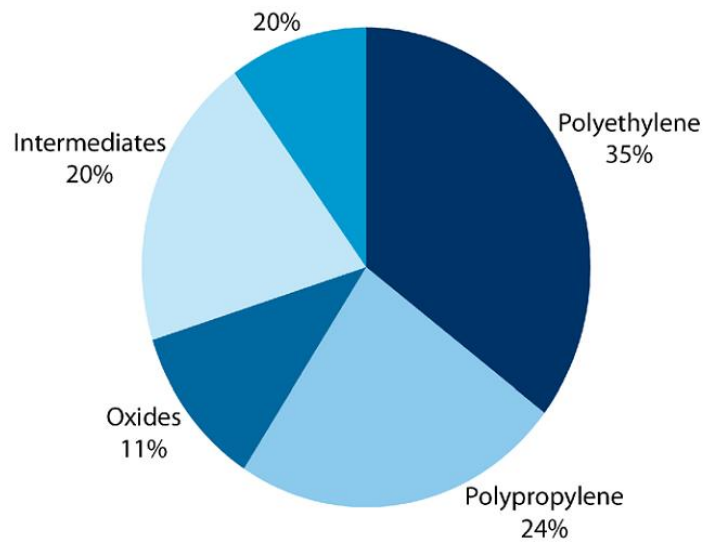


Figure 1.1. Total Consumption of light olefins 205 M ton [7].

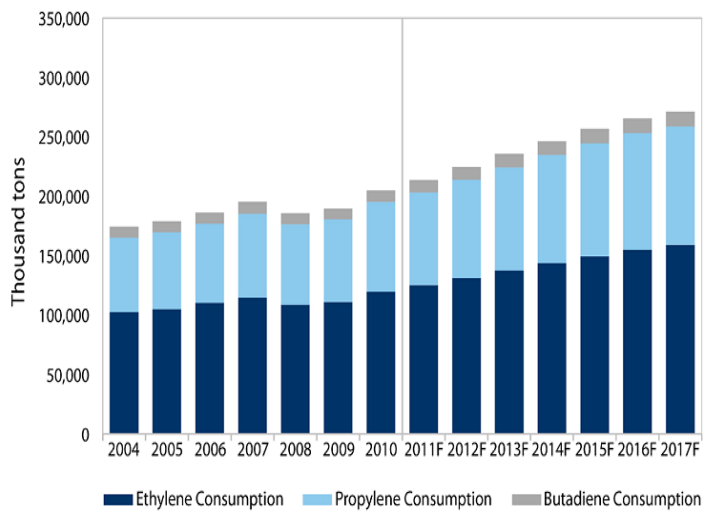


Figure 1.2. Recorded and forecasted Light Olefin Consumption for the period 2004-2017 [7].

1.2 Conventional routes for C4-Olefins production

Fluid catalytic cracking (FCC) is the main commercial method for the production of C4-olefins; as it accounts for about 69% of total C4-olefins production [5]. In FCC process heavy feedstock is converted in the presence of fluidized-bed catalyst; which not only increases the selectivity of the product but also lowers the reaction temperature. As the feed to FCC unit is heavy residue so the product contains fraction of different hydrocarbons. FCC is a nonselective method for the production of C4-olefins and usually, operated above ≥ 550 °C temperature. This process has the following drawbacks: the reaction is highly endothermic, although operated at lower temperature compared to steam cracking process (800 °C) but still requires considerable amount of heat to maintain the reaction at the desired rate, beside this the catalyst deactivation by the coke formation and subsequent catalyst regeneration problems are also very common [8].

The steam cracking is also one of the traditional method used for the production of C4-olefins; it accounts for about 22% of grass C4-alkenes production [5]. The feed to the steam cracker contains water and one of the following hydrocarbon: liquefied petroleum gas (LPG), Naphtha, or ethane. In the typical steam cracking process, a preheated feed is thermally cracked inside the tube furnace which is normally operated at temperature more than 800 °C and at atmospheric pressure to fulfill the energy requirement for the endothermic cracking reaction. The mixture of hydrocarbon fractions are quickly quenched, and then subjected to the expensive separation processes. Ultimately, the C4-olefins are obtained as a side product from this manufacturing method.

The drawbacks of using steam cracking process are: reaction is highly endothermic thus operated at very high temperature and requires adequate amount of heat input to get the optimum yield of the product. Secondly, large amount of coke formation at high temperature causes frequent plant shutdown [8].

Catalytic dehydrogenation is a selective commercial method used on a scale (4% C4-olefins production) for the production of C4-olefins [5]. It mostly uses a fixed bed reactor incorporated with selective catalyst. The general desired reaction for the catalytic dehydrogenation of alkanes is represented by Equation 1.1. The alkane molecules react on the surface of the catalyst to give corresponding alkene along with the formation of H₂ molecule. The reactivity of the dehydrogenation catalyst is directly proportional to the reaction temperature [1].



Dehydrogenation reactions are considered as important alternative for the conversion of propane and n-butane but they are not feasible in the case of ethane due to the high thermodynamic constraints required for the ethylene production (requires temperature greater than 800 °C) [1]. Catalytic dehydrogenation reactions also suffer from same drawbacks of high heat input because of endothermic nature of the reaction, catalyst deactivation, and high thermodynamic constraints [9]. The C4-olefins production from these three conventional routes are summarized by the Figure 1.3.

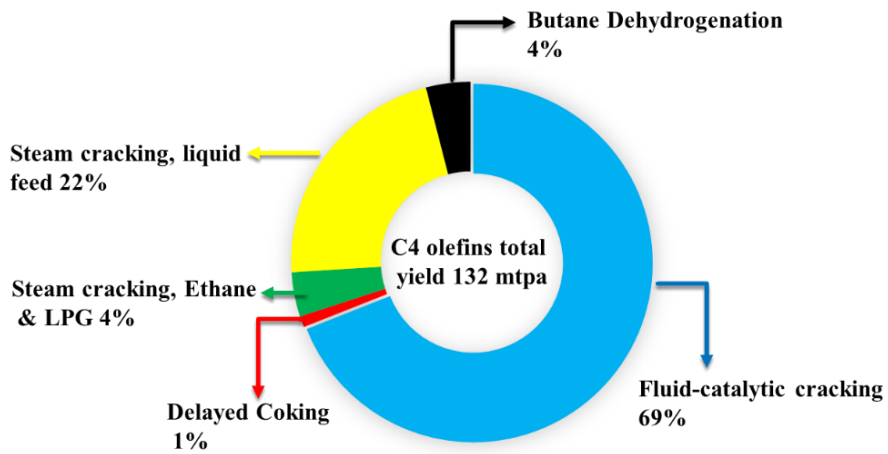
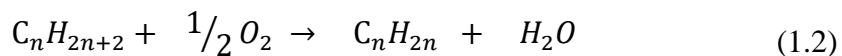


Figure 1.3. Global volume of C4-olefins by process types [5].

1.3 Oxidative Dehydrogenation (ODH)

There are other methods for the synthesis of C4-olefins as well and among these alternative methods ODH is one of the most promising and popular among the researchers in the field of catalysis. The ODH is simply a catalytic dehydrogenation reaction that occurs in the presence of oxide catalyst and/or in the presence of gas phase oxygen. The desired products of ODH reactions contain: alkene and H₂O instead of H₂ which is formed in the catalytic dehydrogenation of alkanes. Two types of ODH reactions are reported in the literature; the first type is carried out in the presence of gas phase oxygen while other one is the novel approach that uses lattice oxygen of catalyst and is carried out in the absence of gas phase oxygen. The general desired reactions for both types of ODH reactions is shown by the Equations 1.2 and 1.3 while their typical process schematic is represented by Figures 1.4 and 1.5 respectively [10,11].



ODH reactions are straight forward; a feed is injected into the reactor which will be either fixed-bed or fluidized-bed depending on the type of ODH reaction. The alkane feed is activated at the particular temperature on the surface of the oxide catalyst, and as result the alkane is converted to an alkyl radical, which on further dehydrogenation either on the catalyst surface (heterogeneous) or in the gas phase (homogeneous) gives corresponding alkene along with the formation of H₂; the hydrogen further reacts with either the lattice oxygen of the catalyst or with the gas phase oxygen to give stable H₂O molecule [1]. The reduced catalyst is again oxidized with the supply of the air and is used

again. It is worth mentioning that the reactions represented by Equations 1.1, 1.2, and 1.3 are ideal reactions, because in the actual ODH reactions the formation of the side products also take place. The undesired reactions that lead to the production of CO_x can be seen in the Figures 1.4 and 1.5. CO_x formation may be due the non-selective complete oxidation of the n-butane and/or further oxidation of the desired products. It is reported that the novel ODH reactions under anaerobic condition successfully retards these side reactions and that in turn could increase the selectivity of the desired products.

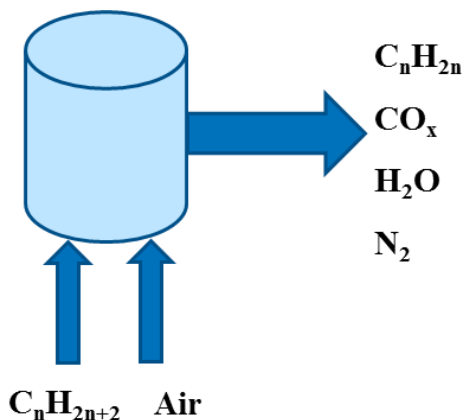
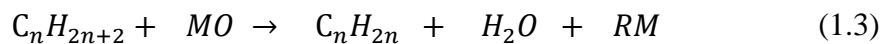


Figure 1.4. Schematic of Fixed-bed ODH in the presence of gas phase oxygen.



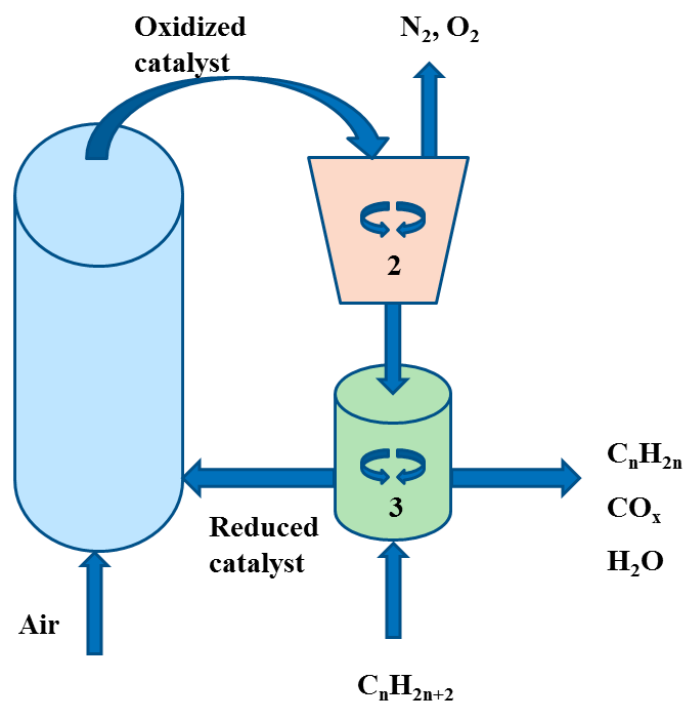


Figure 1.5. Novel gas phase oxygen free ODH schematic.

The nature of the reaction in both types of ODH processes are same that is catalytic selective oxidative dehydrogenation but they differ in some aspects that are: the former involves fixed-bed operation while the latter is usually carried out in the fluidized-bed reactors, the earlier uses gas phase oxygen while the later only uses the lattice oxygen of the oxide catalyst, in the former products are diluted with the nitrogen gas while the second type is free of nitrogen. In conclusion the gas phase oxygen free ODH is far better than the its counter type of ODH; in this work that gas phase O₂ free type of ODH will be used as represented by Figure 1.6 [11].

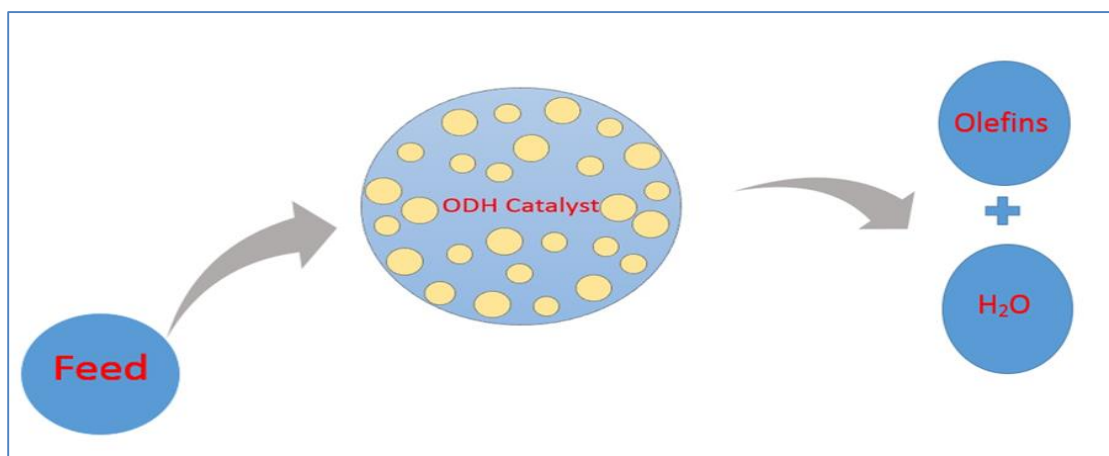


Figure 1.6. Gas phase O₂ free novel ODH.

1.3.1 Motivation for using Novel ODH

Now, let's compare commercial processes with ODH and find out why ODH is far better than the already available manufacturing method of C4-olefins. Figure 1.7 summarizes the drawbacks associated with the commercial methods.

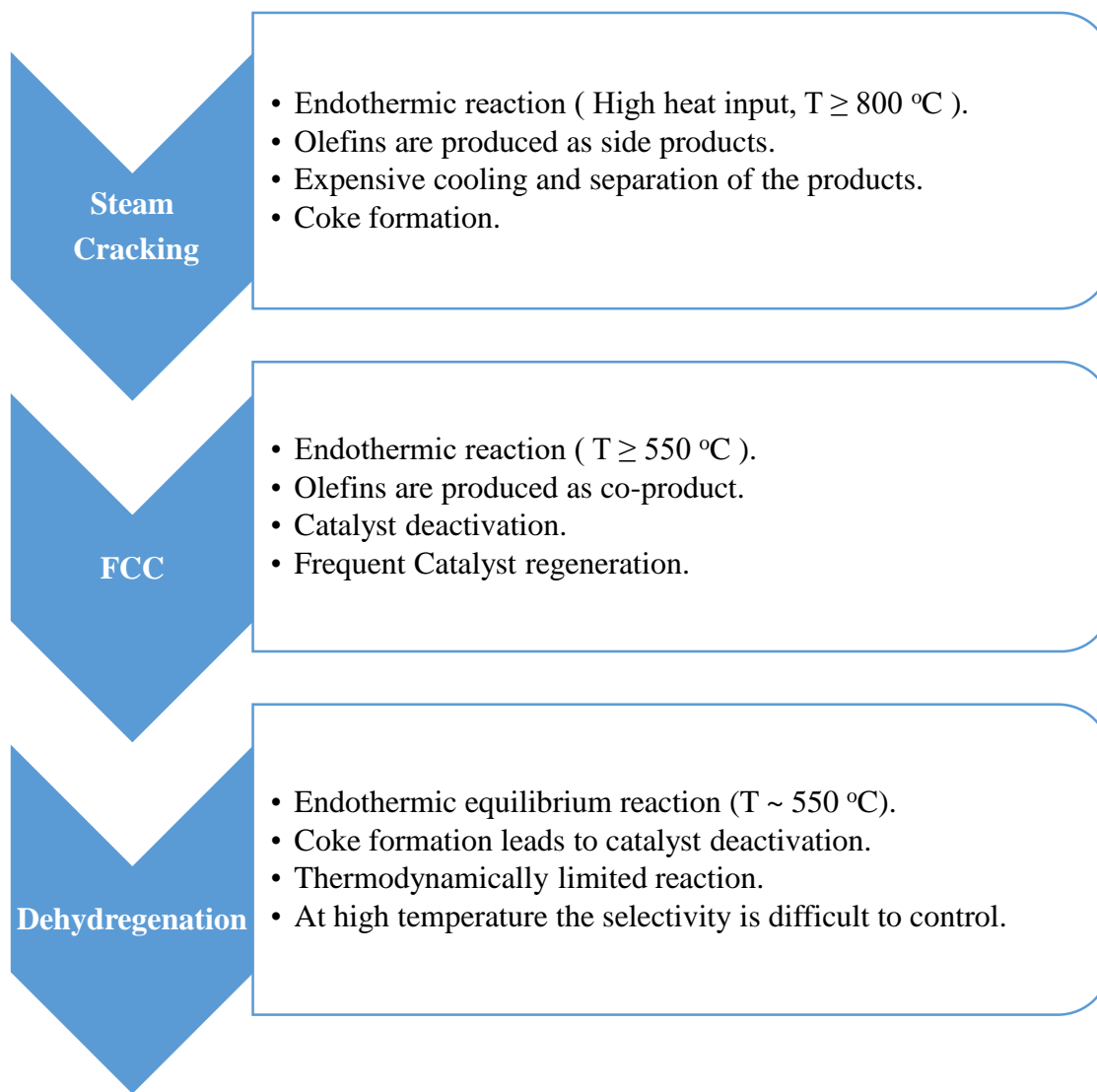


Figure 1.7. Drawbacks associated with the traditional routes for C4-olefins production [8].

Beside these drawbacks the current commercial methods are also non-economical and not environmentally friendly as well; in addition, they are not sufficient to meet the increasing demand for the C4-olefins. This is because of the fact that these conventional routes are usually non-selective in nature: that is they are not on purpose method designed specifically for the production of specific light alkenes but rather the alkenes appear as the side product along with the other hydrocarbon fractions.

Following are the incentives of using ODH over the commercial routes [9,10]:

- i. ODH reactions are exothermic in nature.
- ii. It has limited thermodynamic constraints because of the formation of stable product (H₂O).
- iii. ODH reaction has large positive equilibrium constant value, so practically 100% conversion is possible.
- iv. There is less coke formation on the surface of the ODH catalysts due to the presence of oxygen: which reacts with the coke; thus, catalyst is automatically regenerated and has a longer time on stream value (TOS).
- v. Normally operated at much lower temperature and because of the exothermic nature of the reaction less energy is required for the reaction.

In conclusion, it is decided to synthesize fluidizable Ceria doped $\text{VO}_x/\gamma\text{-Al}_2\text{O}_3$ catalyst for the gas phase oxygen free ODH of n-butane to C4-olefins (sum of 1, iso, cis-butene and 1, 3-butadiene). The major contributions of the present research are:

- i. Synthesized high surface area Mesoporous $\gamma\text{-Al}_2\text{O}_3$ support which is thermally stable up to 800 °C.
- ii. Developed Ce doped fluidizable $\text{VO}_x/\text{Ce-MAs}$ catalysts suitable for gas phase oxygen free ODH reactions.
- iii. Established the phenomenological kinetics involved in the anaerobic ODH of n-butane.

CHAPTER 2

LITERATURE REVIEW

Oxidative dehydrogenation provides a very promising alternative route for the production of unsaturated hydrocarbons mainly because of the formation of stable molecule of water in the product side. Thus, practically complete conversion is possible even at the low temperature and pressure [1,12]. Further, ODH reactions are also less subjected to catalyst deactivation by coke formation and cracking due to the irreversible exothermic nature of the reaction. Despite these incentives of ODH over the commercial methods, it has some shortcomings [13]: due to the exothermic nature of ODH, it may require extensive care in the operating conditions, secondly presence of the reducible species in the reactor may cause the nonselective reactions which lowers the yield of the C4-olefins e.g., reaction with gas phase or lattice oxygen could result in oxygenated hydrocarbons, degradation products and above all combustion products (CO_x). These side reactions may be thermodynamically more favorable. In fact, it is reported by [1] that olefins are more susceptible to homogeneous gas phase reactions than alkanes thus imposing a upper bound on the yield. So it turns out that higher selectivity is usually attained at lower conversion. But operation at lower conversion requires expensive product separation and recycling of the unreactive feed. In order to address this challenging low yield issue, extensive research has been going on to find out the most selective catalyst for ODH of n-butane. The reaction pathways are further elaborated by kinetic modelling that helps in understanding the reaction mechanism.

2.1 Type of the catalyst system used for the ODH of Butane

As n-butane has more no. of secondary C-H bonds than either ethane or propane thus it exhibits higher rate of homogeneous reaction with the gas phase oxygen. For example, ODH reactions in 5 cm³ reactor in the presence of oxide catalyst typically needs 500 °C temperature for the ODH of n-butane while propane requires 550 °C temperature [14].

Oxidative dehydrogenation of butane has been studied over different varieties of the catalysts, ranging from single metal oxide, supported metal oxide, and promoted metal oxides. In most of the cases it has been reported that the promoted metal oxide works better than the un-promoted metal oxide [12]. The reaction temperature reported ranging from 400 to 550 °C and almost all of the ODH reactions were carried out in the presence of the gas phase oxygen. While in fewer cases the anaerobic novel ODH approach was utilized. According to [15] the ODH catalysts for n-butane can be classified in to the following three categories:

1. Unsupported catalysts.
2. Supported catalysts.
3. Promoted catalysts.

2.2 Unsupported catalysts

The earlier studies of ODH of butane were mostly conducted on the unsupported catalysts and among these V-Mg oxide is particularly important, as these metal oxides being used frequently for the ODH of n-butane [1,14,16–20]. The initial step in the activation of n-butane ODH reactions is the dissociation of secondary C-H bond, while minor contribution is also from the cleavage of the primary C-H bond. When the activity of light saturated hydrocarbons were compared over the V-MgO catalyst, the following order of increasing activity of the alkanes was observed: ethane < propane < n-butane. The main reason behind such reactivity is the no. of secondary carbon atoms present in the particular alkane. The more the no. of secondary carbon atoms in the alkane, the higher will be the rate of that reaction [14].

The selectivity of C4-olefins depends on the relative wt% of vanadia, MgO and on the method of their synthesis as well. It was reported that catalysts containing intermediate (10-60%) wt% of vanadia are very selective than the one having too small or too large wt% of vanadia [21]. As for the synthesis method, it is recommended to use magnesium carbonate as the precursor of MgO instead of magnesium hydroxide, while ammonium carbonate as a dehydrating agent is reported to work better than potassium hydroxide [1]. Based on the catalyst characterization results, the active and selective phase in V-MgO catalysts is $\text{Mg}_3(\text{VO}_4)_2$ having isolated tetrahedral crystal geometry [20].

The selectivity of the other orthovanadates, e.g. nickel, iron, cobalt, chromium, zinc, neodymium, copper, and europium were investigated by [22–24]. An inverse trend was found between the selectivity and the reduction potential of the cation, thus $\text{Mg}_3(\text{VO}_4)_2$ having lowest reducibility, exhibits highest C4-olefins selectivity (60% selectivity of

butane + butadiene at 500 °C) while copper orthovanadate shows lowest selectivity (5% selectivity of butane + butadiene at 500 °C) but represents higher conversion due to lower reduction potential.

A comprehensive study was done by [25,26] on Ni-MoO₄ catalysts for the ODH of butane in presence of the gas phase oxygen. It was found that by doping Ni-MoO₄ with more basic IA elements, tends to increase the selectivity of the desired products while the activity of the catalyst follows the opposite trend. The basicity increases linearly with the amount of the dopant [25]. In the separate study by [26], it was revealed that IIA group elements when used as dopant for Ni-MoO₄ catalyst works even better than the IA elements [26]. Further, the catalyst treated by deposition-gasification prior to coke formation works better than the freshly prepared catalyst [26].

The ODH of butane was also studied over the transition metal oxides promoted zeolites , zinc-iron [27], zinc-manganese [12], magnesium-vanadia [28] and supported oxides of vanadium, nickel, molybdenum [29].

2.3 Supported catalysts

The metal support interactions and acid base nature of the support is one of the key factor determining the product selectivity [18]. Vanadia and nickel oxide are the two most utilized active metal phases and they are normally impregnated on Al₂O₃, silica, MgO, MCM-41, ZrO₂, Ti-HMS, USY, and NaY [30–36] etc. The magnesium oxide is reported to be very good support for vanadia due to the alkaline nature of the support, but it's not an ideal support material due to its lower BET surface area and lower mechanical strength [19].

The physio-chemical properties of γ - Al_2O_3 makes it very active catalyst support material for the ODH of butane. However, lower dispersion of the active metal oxide phase was observed on that support due to its strong acidic nature [24]. In order to lower the acidity of alumina, it is usually modified by group IIA elements namely: Mg, Ca, Sr, and Ba. It was found that the γ - Al_2O_3 doped with Ca, Sr and Ba shows lower rate of reaction while the Mg modified alumina represent highest activity and selectivity giving 64.3% butene selectivity with 30.3% conversion at 600 °C [34].

In the separate study, vanadium oxide was impregnated on different support materials, e.g. α - Al_2O_3 , γ - Al_2O_3 , USY, NaY [30], and the catalytic performance was evaluated for the gas phase oxygen free ODH of butane over these catalysts. The VO_x /USY catalyst came out to be most active and selective due to its lower acidity. Beside basicity of the support material, the different amount of VO_x impregnated on the oxide support give rise to different surface species, usually higher vanadium loading (>10% wt) results in the formation of crystalline V_2O_5 phase which is reported to be non-selective for ODH of butane [37].

The high surface area mesoporous silicate (MCM-41) was also implied as a support material for the VO_x [33]. The important finding of this research was that lower loading of VO_x retains the mesoporous structure of the support while at higher loading the structure collapses due to increase in the acidity. Similarly the effect of vanadium precursor on the surface area of the USY-zeolite revealed that the acidic precursor damages the structure and reduces the surface area so it was recommended to use basic precursor for vanadium such as: ammonium acetyl acetone [36].

The combination of magnesium oxide and aluminum oxide when used as support for MgMoO_4 catalyst gives promising C4-olefins yield when the ODH reaction were performed in the absence of the gas phase oxygen. The reaction occurs by taking lattice oxygen from the catalyst surface but this operation need fluidized-bed reactor [12].

2.4 Promoters

Several catalytic promoters were also implied to increase the performance of the ODH catalysts. The most notable one are K, Cs [38], and $\text{Cr}_2\text{O}_3/\text{TiO}_2$ [31], used to enhance the activity of Ni/Sn/P-O, magnesium molybdate and vanadia magnesium oxide catalysts, respectively.

Alkali and alkaline earth metals were also extensively used in the literature to decrease the acidity of the support material. The rate of formation of olefins seemed to depend on the reducibility of the surface species of the catalyst while the selectivity to corresponding olefins showed inverse trend to the activity [25]. Among alkali metals Cesium is reported to be more effective in its group while in alkaline earth metals works even better than IA group elements, addition of both increases the selectivity of butadiene [15].

2.5 Kinetic Modeling

The increasing demand for the C4-olefins led the researchers to do significant work to improve the alternative methods (ODH of butane) for the production of these olefins [1,12,18], but at same time, lesser contributions were made towards the kinetics studies of these reactions. In fact, most of work is mainly based on the VO_x catalysts or more specifically VMgO mixed oxide catalysts [16,39–41].

In the kinetics of butane ODH different kinetic models viz, Mars van Krevelen (MK), Eley-Rideal (ER) and Langmuir-Hinshelwood (LH) were tested to verify the proposed reaction pathways. In most of the cases pure butane was assumed as the starting material but with this assumption, when the experimental data was fitted into either LH or ER, some discrepancies' in the predicted values were observed.

The modification in the MK method proposed by [41] works very well in the gas phase oxygen free condition. The rate of reaction in such situation also depends on the degree of catalyst reduction. It was proposed by [41] to assume two reducible surface species on the catalyst surface namely: θ and λ , where the first one was assigned to the production of both selective and nonselective products while the later was only attributed to production of nonselective reactions. These modification in the MK model leads to very high coefficient of fitting with good confidence interval.

Similarly, [16] studied the kinetics of the butane ODH reaction in gas phase oxygen free condition, using MK reaction mechanism. Two types of surface oxygen species were considered: lattice oxygen and loosely bond surface oxygen, the first type promotes both the desired reaction and undesired reaction while the later was assumed to favor the unselective reactions. The assumption of these kinds of surface species were necessary to explain why the selectivity decreases with the degree of the catalyst decay. Which actually, contradicts the observation that selectivity on freshly prepared catalyst in the presence of gaseous oxygen is smaller than on the reduced catalyst.

It is important to mention that only these [16,39–41] studies were reported in anaerobic condition, considering the MK reaction mechanism. However, no study is

reported in fluidized-bed reactor in anaerobic condition where the experimental data is fitted by LH mechanism for the ODH of n-butane to C4-Olefins that take into the account of catalyst reduction term as well. The incentive of using CREC Riser Simulator are: firstly, isothermal reaction conditions are possible and secondly almost no mass transfer limitations is present due to high fluidization and finally presence of online facility for the reoxidation of the spent catalyst enable its practical implementation at the industrial level. The successful fitting of LH is reported by [42] for the gas phase oxygen free ODH of propane to propylene using $\text{VO}_x/\gamma\text{-Al}_2\text{O}_3$ catalyst in the fluidizable bed batch reactor.

2.6 Motivations

After going through the literature we are motivated to use the vanadium oxide as an active phase because it is recommended in the literature [37] that VO_x is one of the most active and selective catalyst for butane ODH to C4-olefins.

Mesoporous $\gamma\text{-Al}_2\text{O}_3$ (MAs) is very important because of its use both as catalyst and catalyst support in the fields of petro-chemical industries, waste-water treatment, adsorption, ceramics, biomedical and in electronics [43]. $\gamma\text{-Al}_2\text{O}_3$ has this favor due to its unique textural and chemical characteristics such as: high BET surface area, uniform pore size distribution, high mechanical and hydrothermal stability and large pore size volume [44,45], that's why the synthesis of MAs is still the focal point of many researchers in order to acquire more promising properties [46–48]. Above all, VO_x when impregnated on this support exhibits highest catalytic activity [36].

Among the rare earth metal oxides, ceria (CeO_2) is of the paramount importance due to its tri-functional catalytic nature and its use in the pollution control, absorption, deep combustion, gas detection and in fuel cells [49–52]. The catalytic behavior of CeO_2 can be further modified either by impregnation or incorporation it on the Mesoporous structure of $\gamma\text{-Al}_2\text{O}_3$. It is believed that this doping will result in a twofold advantages that is the incorporation will increase the structural stability of $\gamma\text{-Al}_2\text{O}_3$ while in turn CeO_2 will become more active on the Mesoporous frame-work [53]. This feature makes its use in the field of catalysis [54].

2.7 Conclusion of Literature Review

From Table 2.1, one can see that most of the work has been done in the fixed bed reactor and different combination of catalyst has been used ranging from metal oxide, supported metal oxide, and promoted metal oxides. In most of the cases the promoted metal oxide works better than the non-supported metal oxide. The reaction temperature ranging from 400-550°C and in almost all of the cases gas phase oxygen is blended with the feed.

In some cases, instead of oxygen CO_2 is used as the soft oxidizing agent. By using CO_2 the product selectivity increases to great extent because of the suppression of the homogeneous gas phase complete combustion of alkyl radical. In order to use CO_2 as the oxidizing agent the reactor temperature should be increased up to 100 °C as compared with using O_2 as the oxidant. This is because of the strong bonding of oxygen with the carbon atom in CO_2 [3,32,55]. Water can also be mixed with the feed to increase the selectivity of C4-olefins and in most of the ODH reaction if oxygenated products are the desired products then addition of water to the feed is necessary because it tend to react with the intermediate

alkyl radical to form oxy-alkyl radical which on further oxidation gives oxygenated products [18].

After going through this literature we concluded that as limited work has been done for the novel ODH of n-butane in a gas phase free oxygen environment by using VO_x catalyst supported on the Mesoporous frame work of $\gamma\text{-Al}_2\text{O}_3$ and further the support will be modified by doping ceria. This combination has never been studied before and it is expected to work better than $\text{VO}_x/\gamma\text{-Al}_2\text{O}_3$ because as Mesoporous structure of $\gamma\text{-Al}_2\text{O}_3$ will be used so more surface area will be available for the reaction and this will increase both the conversion and selectivity. The presence of ceria will not only increase the thermal stability of the catalyst but will also prolong the activity of the VO_x by reducing the deactivation of the catalyst due to unique oxygen storage/release characteristics and redox nature of it [51,52]. Further, the reaction will be performed in anaerobic condition so, better control over the selectivity would be possible and above all effect of fluidization will increase the conversion by reduce the mass transfer limitations.

Table 2.1. Summary of the literature review

Reference	Catalyst type	Temp °C	Selectivity/ Conversion	Reactor type
Bing Xu et al, 2015	V ₂ O ₅ /MO-Al ₂ O ₃ (M = Mg, Ca, Sr, Ba)	600 °C	64.3% /30.3%	Fixed bed
X. Wang, et al 2015	VO _x / MCM-41	550 °C	57% / 47.4%	Tubular reactor
B. R Jermy et al. 2015	Bi-NiO _x /γ-Al ₂ O ₃	450 °C	47% / 7%	Fixed bed CSTR reactor
E.M. Garcia et al 2005	VO _x / USY Zeolite	520 °C	75% / 8%	Fixed bed reactor
M. Volpe et al 2004	VO _x / X (X = USY, NaY, α-Al ₂ O ₃ , γ-Al ₂ O ₃)	520 °C	68% / 8%	Fixed bed reactor
Raju. G, et al 2014	VO _x /CeO ₂ -ZrO ₂	600 °C	50.2% / 30%	Fixed bed
Yan. W, et al 2014	Fe ₂ O ₃ / Al ₂ O ₃	600 °C	21% / 77%	Tabular reactor
Optics, P. N et al, 2007	P-oCNTs	450 °C	22%	Tabular reactor
Wang, W, et al, 2014	V-Mg-0	480 °C	68%	Fixed bed
Trovarelli, A, et al, 2007	Ni-Mo-P-0	482 °C	75%	Fixed bed
Cai, W., et al 2010	Mg-Ni-Sn-0	482 °C	51%	Fixed bed
Rahmani, S et al, 2014	Mg-Ni-SO ₄	538 °C	58%	Fixed bed
Fahim, M., et al 2009	Mg ₃ (VO ₄) ₂ /MgO	450 °C	40.5%	Fixed bed
Lee, H., et al 2012	Ni-P-O	538 °C	70%	Fixed bed

CHAPTER 3

OBJECTIVES

3.1 Main Objectives

The main objective of this research is to develop a Ce doped fluidizable VO_x/Ce-MAs catalyst suitable for the oxidative dehydrogenation of n-butane to butene under gas phase oxygen free conditions. It is also the objective to establish mechanism based kinetic model representing the n-butane ODH using the lattice oxygen of the catalyst.

3.2 Specific Objectives

- i. To prepare high surface area meso γ -Al₂O₃ (MAs).
- ii. To synthesize Ceria promoted VO_x/MAs catalysts.
- iii. To characterize the synthesized catalysts using various physicochemical characterization techniques such as: BET surface area, XRD, TPR, TPD, SEM-EDX, FTIR, and Raman.
- iv. To evaluate the promising catalysts in a laboratory scale fluidized bed reactor under gas phase oxygen free reaction conditions using n-butane as feed.
- v. To evaluate the effect of the Ceria loading on the catalytic behavior of VO_x for the ODH reaction of butane.

- vi. To find the optimum conditions for the best selectivity of C4-olefins based on the yield of the product.
- vii. To evaluate the catalyst stability and reactivity in the operating condition range.
- viii. To establish a kinetic based mathematical model for the ODH of n-butane reactions in anaerobic fluidized-bed conditions.

CHAPTER 4

EXPERIMENTAL PROCEDURE

4.1 CATALYST SYNTHESIS

4.1.1 Catalyst Preparation

In this work, both MAs and Ceria modified MAs were prepared by modifying the approaches given by the X. Shang et al [56] and J. Wang et al [57]. In this typical surfactant free approach, $\text{Ce}(\text{NO}_3)_3 \cdot 6\text{H}_2\text{O}$ is added in Al-precursor solution which is then partially hydrolyzed by Ammonium carbonate solution and then calcined at 400 °C. The crystalline modified Ce/MAs support thus obtained, exhibits higher BET surface area, uniform pore size distribution and better thermal stability.

4.1.2 Chemical used

Aluminum nitrate nano-hydrate, Cerium nitrate hexa-hydrate and Vanadium acetylacetonate were obtained from Sigma-Aldrich and used without further purification. Ammonium carbonate was purchased from Fisher limited and Deionized water was used in chemicals preparation. The glassware was first washed with HNO_3 , then rinsed with deionized water and finally dried before use.

4.1.3 Support preparation

$\text{Al}(\text{NO}_3)_3 \cdot 9\text{H}_2\text{O}$ (37.5g) was dissolved in deionized water (50ml), and then $(\text{NH}_4)_2\text{CO}_3$ (1M) solution was added drop wisely into the Al-precursor solution under vigorous stirring (Heating magnetic stirrer with timer, Arec. T) until the formation of polymeric gel having PH of 5.3. The gel was dried in the oven at 30 °C for 24 h, and then aged at 150 °C and 200 °C each for 12 h interval at the ramping rate of 1 °C/min. Finally calcined at 300 °C for 12 h at the ramping rate of 1 °C/min.

4.1.4 Synthesis of Ceria/MAs

The method of the formation of Ceria doped MAs is the same as that of MAs support but before the hydrolysis step, appropriate amount of (0.2, 1, 3, & 5 wt%) $\text{Ce}(\text{NO}_3)_3 \cdot 6\text{H}_2\text{O}$ is added in the Al-precursor solution, here the calcination temperature is set as 400 °C for 6 h. The product of calcination is named as Ce-MAs. In the typical synthesis of 1% doped MAs, 1.16 grams of Ce-precursor was dissolved in 10 ml of deionized water and then added to the Al-precursor solution under vigorous stirring condition. The mixture was partially hydrolyzed by one-molar ammonium carbonate solution until the formation of white precipitates. The obtained gel was dried in the oven at 30 °C for 24 h, and then aged at 150 °C and 200 °C each for 12 h interval at the ramping rate of 1 °C/min. Finally, calcined at 400 °C for 12 h at the ramping rate of 1 °C/min.

4.1.5 Active site preparation

VO_x is impregnated on both the Ce-MAs and MAs using excessive solvent impregnation method under vacuum condition. The $\text{VO}_x/\text{Ce-MAs}$ synthesis method involves the following five steps:

1. Active site wet impregnation
2. Filtration
3. Drying
4. Reduction
5. Calcination

On both MAs and Ce-MAs supports, vanadia content is kept at 5 wt%. In the typical impregnation of 5 wt% of VO_x on the 0.2 wt% Ceria modified MAs, 0.86 gram of vanadium acetylacetonate was dissolved in excess amount of toluene. The resultant VO_x -precursor solution was added drop-wisely into 3 gram of Ce-MAs solid support under vigorous stirring condition. The solution was stirred for 6 h under vacuum mode and then filtered. After the filtration the solid residue was allowed to dry at the room temperature for 24 hours and then further dried in the furnace at 140 °C at a ramping rate of 0.5 °C/min for additional 6 hours. Upon drying the prepare material was reduced in fluidizable bed reactor. The source of fluidization and reduction was 10 % H_2 with balance Helium gas mixture. The bed temperature of the dried catalyst was raised from the ambient to 750 °C at a ramping rate of 0.5 °C/min and held constant at 750 °C for additional 8 h. Upon completion of the reduction step the catalyst was oxidized in the furnace at 750 °C using

the same ramping rate and time interval employed for the reduction step. For the sake of simplicity the synthesized catalysts will be named as follows:

Table 4.1. Synthesized catalysts and their nomenclature

S.No	Samples	Nomenclature
1	5 wt% VO _x /0.2 wt% Ce-MAs	0.2 Ce
2	5 wt% VO _x /1.0 wt% Ce-MAs	1.0 Ce
3	5 wt% VO _x /3.0 wt% Ce-MAs	3.0 Ce
4	5 wt% VO _x /5.0 wt% Ce-MAs	5.0 Ce

4.2 Catalyst Characterization

The desired ODH catalyst should have higher surface reactivity for the selective reaction as well as high product yield. The catalyst characterization is an important part of the catalyst evaluation and development. Important piece of information about the physiochemical properties as well as structural and relative concentration of different phases can be extracted from different characterization results. Among different physico-chemical properties, catalyst active surface area, loading of active metal oxide, thermal stability of the catalyst, oxygen uptake, and degree of reduction of active phase, degree of metal oxide dispersion, surface acidity and structure of the surface metal oxides are of the paramount importance. The following state of art characterization techniques will be used for the evaluation of the catalyst.

1. Field emission Scanning Electron Microscopic analysis (FE-SEM).
2. Energy dispersive X-rays analysis using SEM (SEM-EDX).
3. X-ray diffractometry (XRD).
4. Raman Spectroscopy.
5. Fourier transform infrared spectroscopy (FTIR).
6. Thermogravimetric analysis (TGA).
7. NH₃-Temperature programmed desorption (NH₃-TPD).
8. Temperature programmed analysis (H₂-TPR & TPO).

In the subsequent section of this chapter the theory and operating procedure will be discussed for these characterization techniques.

4.2.1 Field emission scanning electron microscopy (FE-SEM)

The morphological and elemental analysis of the synthesized catalysts were carried by field-emission scanning electron microscope on FE-SEM, JSM-6500F, JEOL and LYRA 3 Dual Beam, Tescan equipped with energy dispersive X-Ray spectrometer (EDX, Oxford instrument). Samples were coated with gold prior to FE-SEM imaging and for the quantitative analysis the accelerating voltage of 30 kv was used.

4.2.2 X-ray diffraction (XRD) analysis

X-ray diffraction is one of the primary techniques used to determine physico-chemical make-up of crystalline solids. It is also called X-ray powder diffraction. Sometimes the technique is referred to as X-ray powder diffractometry. Name of instrument is X-ray Diffractometer (XRD). The applications of XRD technique are: determination of crystal structure (arrangement of atoms, lattice parameters), Identify compounds, Identify different phases in a compound/sample, Relative concentration of phases/compounds, Crystallite size measurement, Crystallinity, Residual Stress measurement, Crystal orientations, and Study of phase equilibria [58].

X-ray powder diffractometry (XRD) was conducted to identify and find the relative concentration of the crystalline phases present in VO_x-Ce/MAs and VO_x-MAs catalysts. Mini-Flex II bench top XRD System from Rigaku with Cu-K_α radiation source was used to analyze the prepared catalyst and supports. The other operational parameters were: wavelength = 0.15406 nm, 30 kV, 15 mA and a normal scan rate of 3° scan per minute with the 2θ range of 10-90 degrees with a step size of 0.02.

4.2.3 Raman Spectroscopy

Raman spectra were recorded using Horiba Raman spectrometer (iHR 320) with CCD detector, which eliminates the elastic beam scattering. The excitation wavelength of 532 nm with the laser intensity of 50% at 50-2500 spectrum was used in all the cases. All the catalysts were dehydrated at 500 °C for 1 h before their spectra collection.

4.2.4 Fourier transform infrared spectroscopy (FTIR)

FTIR characterizes the infrared spectrum of absorption, transmission or photoconductivity through a solid or liquid in order to find out the nature of the functional groups attached to a particular support. FTIR of the prepared samples were conducted by using Nicolet 6700 Thermo Fisher Scientific instrument. For each experimental run, 3 mg of the catalyst is thoroughly mixed with 400 mg of standard KBr. The range for the collection of the excited FTIR spectrum were 400-4000 cm^{-1} .

4.2.5 Thermogravimetric analysis

This technique is used for checking the physical and chemical stability of the catalyst as function of increasing temperature. If catalyst contains any low boiling material that will evaporate and will appear as peak in the derivative of the weight loss vs temperature graph. TA SDT-Q600 model of the TGA equipment is used for the analysis. The operation is straight forward just place the sample in the crucial and then decomposed it by setting the target temperature and ramp rate. The operating parameters were: heating ramp 20 $^{\circ}\text{C}/\text{min}$, weight of the sample 15 mg, temperature range 25-1000 $^{\circ}\text{C}$ and purging rate of Nitrogen was 20 cm^3/min .

4.2.6 Temperature programmed desorption (TPD)

NH_3 -TPD analysis is widely used to determine the total acidity, strength of the acidic sites and, metal support interaction. These experiments were performed on Micromeritics AutoChem-II also used for the analysis of TPR as shown by Figure 4.1. For each experimental run, approximately ~ 100 mg of the sample was placed in a quartz U-tube and flashed under Helium flow rate of 30 cm^3/min for 3 h at 300 $^{\circ}\text{C}$. After this degassing step, the bed temperature was brought back to 100 $^{\circ}\text{C}$ and saturated with 5%

NH₃ (balanced He) gas mixture for 1 h at the flowrate of 50 cm³/min. The unadsorbed NH₃ molecules between the catalyst particles were then removed by purging helium over the catalyst bed at flowrate of 50 cm³/min for 1 h. The NH₃ desorption was recorded with TCD detector by rising the sample temperature to 750 °C with the ramping rate of 10 °C/min.

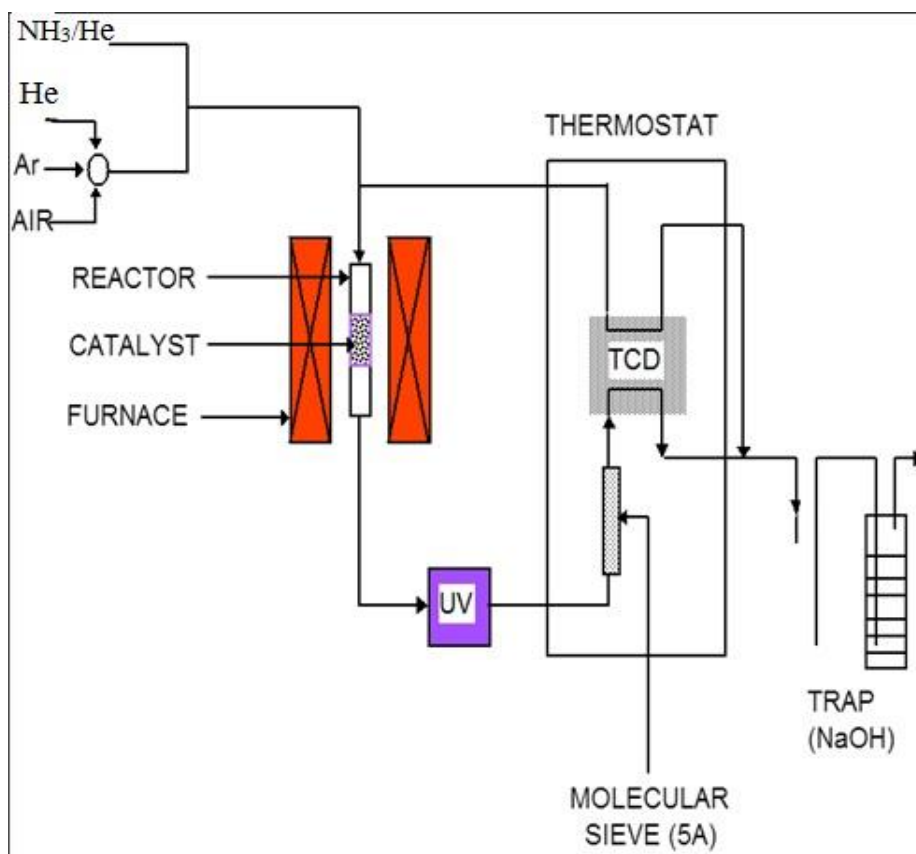


Figure 4.1. Process Schematic for NH₃-TPD characterization, Micromeritics AutoChem-II

4.2.7 Temperature programmed reduction and oxidation (TPR/TPO)

The reducibility and maximum reduction temperature for VO_x/CeO₂-MAs catalysts were analyzed by TPR characterization. Further, the repeated TPR/TPO analysis assisted in the catalyst stability measure. The TPR experiments were performed in the Micromeritics AutoChem-II instrument using a mixture of H₂/Ar (5%) as reducing gas (refer to Figure 4.1). Prior to the reduction the catalysts were pretreated in the flowing Argon (99.9%) at 300 °C for 3 h at flowrate of 50 cm³/min. After cooling to the ambient temperature, the bed temperature was rise to 750 °C at a rate of 10 °C/min in the reducing gas (50 cm³/min). The thermal conductivity detector (TCD) measured the concentration of the exiting H₂ gas. The total H₂ consumption was then calculated by finding the area under the H₂ concentration curve (TCD signal vs time).

4.3 ODH in the CREC Riser Simulator

The anaerobic oxidative dehydrogenation experiments of n-butane over the vanadium oxide supported on the ceria doped MAs catalysts were conducted in CREC Riser Simulator batch reactor [59]. as shown by Figure 4.2. This lab-scale reactor (53 cm^3) is designed for the evaluation and kinetic studies of the catalysts under fluidized bed condition (riser/downer) [8,42,60,61]. The reactor section mainly consists of two parts that are: upper section and lower section. The overall reactor assembly has the following key components: impeller, retaining rings, grids, thermocouples, heaters, and feed injection point. The vacuum box is directly connected with the reactor to take the products after the specified reaction time through a 4 port valve. While these reaction products were analyzed by an online GC connected with the vacuum box through a 6 port valve [26,62].

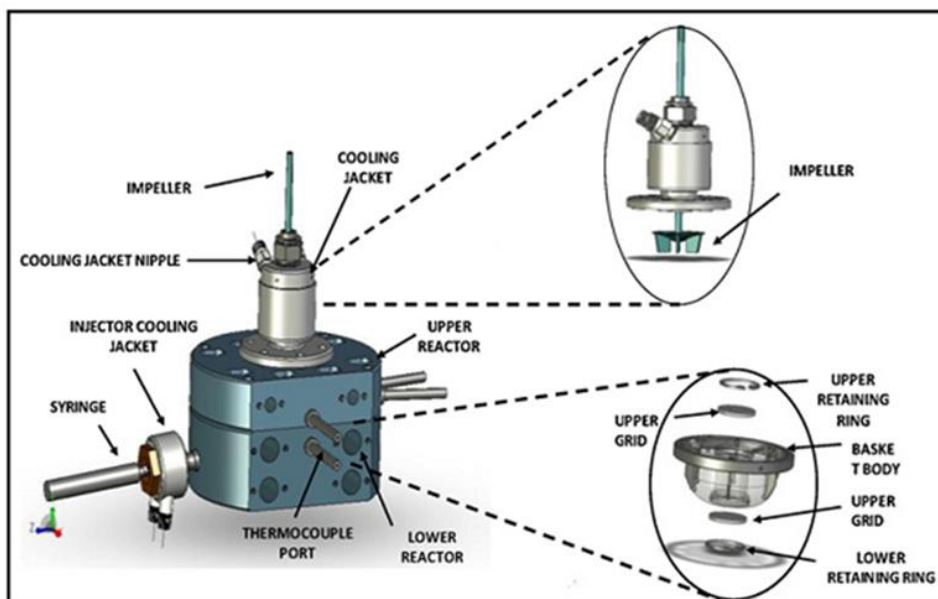


Figure 4.2. CREC Riser Simulator reactor assembly

The complete process flow diagram of fluidized bed batch reactor is represented by Figure 4.3. In each ODH run, the reactor basket was filled with 1.0 g of the catalysts sample and both the reactor and vacuum box were flushed with argon. Prior heating the reactor, both reactor system and vacuum box were subjected to the leak test. After confirmation of no leak in the system, the temperature of the reactor was gradually raised to the desired temperature level, while during this heating process, the system was continuously purged by argon gas in order to avoid interference due to gas phase oxygen. When the reaction temperature reaches to its desired value, the reactor was depressurized to one atmospheric pressure (14.7 psi) by stopping the argon flow and at this desired pressure value the reactor was isolated by isolation valve from the vacuum box. While the vacuum box pressure was further reduced to 20.7 kPa (3.75 psi) with the help of the vacuum pump. At this point, the catalyst was fluidized by rotating the impeller located above the reactor basket and in few seconds, it reaches to the set point speed (4000 rpm). Now, the reactor is ready for the injection thus the feed (n-Butane) was injected into the reactor with the help of the preloaded air-tight syringe. The isolation valve automatically opened after pre-specified reaction time thus allowing the collection of all the reaction products into the vacuum box. An online GC (Agilent 7890A) equipped with FID and TCD detectors were used to analyze these reaction products. The product analysis was repeated three times in order to achieve good accuracy.

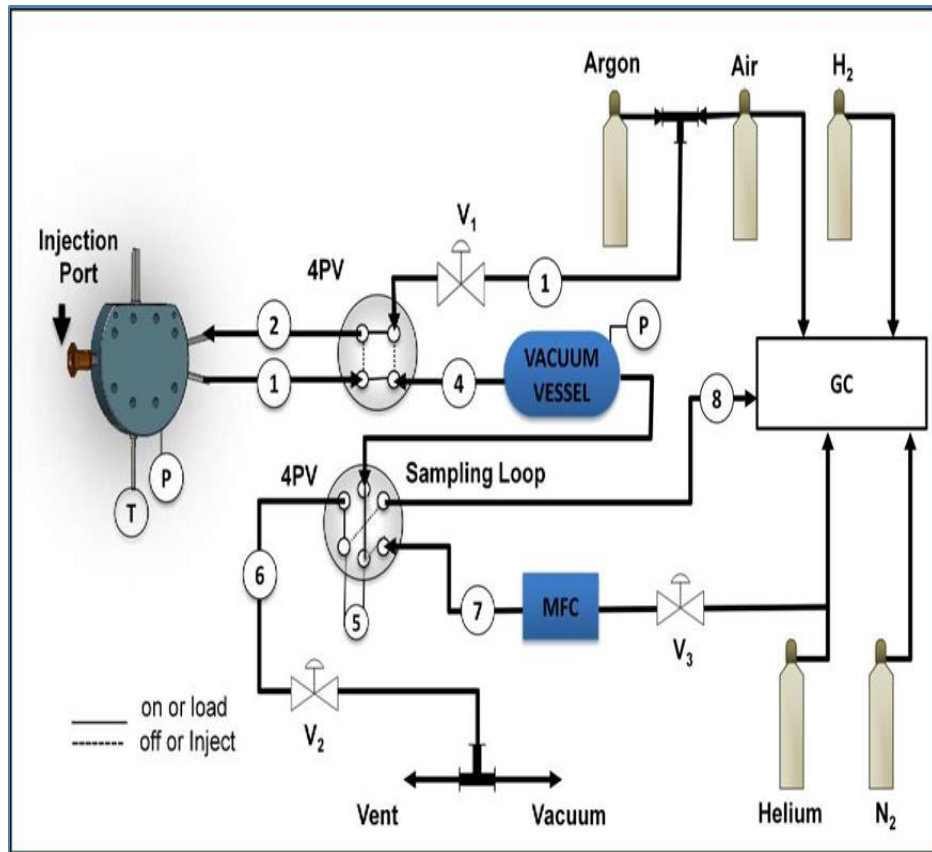


Figure 4.3. Schematic Diagram of the CREC Riser Simulator experimental set-up

The effect of temperature on the selectivity, conversion and yield is studied from 450 °C to 575 °C for the ODH of the ethane in the Riser Simulator fluidized bed reactor. Other operating parameters are kept constant, e.g., impeller speed 4000 rpm, pressure of the reactor 14.7 psi and vacuum box 3.5 psi, and the amount of the feed of ethane at 1 ml, catalyst weight 1 gram. Equations 4.1 and 4.2 were used for the calculation of product selectivity and feed conversion.

$$\text{Conversion, X (\%)} = \left(\frac{\text{Moles of feed reacted}}{\text{Mole of n - butane fed}} \right) \times 100 \quad (4.1)$$

$$\text{Selectivity of product i, } S_i \text{ (\%)} = \left(\frac{\text{Moles of product i}}{\text{Moles of feed reacted}} \right) \times 100 \quad (4.2)$$

CHAPTER 5

RESULTS AND DISCUSSION

In this section of the thesis the results of different characterization will be discussed. The surface morphology and identification of different elements present in the synthesized catalyst will be determined by the FE-SEM and EDX FE-SEM analysis respectively. The presence of crystalline phases, molecular structure, and nature of the function groups attached with the support will be found out by XRD, Raman, and FTIR characterization techniques respectively. While the catalyst reactivity and acid base characteristics will be evaluated by the TPR and NH_3 -TPD techniques.

5.1 Catalyst Characterization Results

5.1.1 FE-SEM analysis

The typical SEM images shows the size and the shape of the freshly prepared catalyst. Figure 5.1 (a) shows the SEM micrograph of the prepared MAs, one can clearly identify the homogeneous mesoporous network of the Gemma alumina. Figure 5.1 (b) represents the SEM image of the 0.2 Ce catalyst and it also shows similar morphology as that of the pure support thus almost maintaining the mesoporous frame work of the support. The white brighter dots represents the VO_x amorphous phase and one can see a good distribution of the VO_x onto this support. It is found that from Figure 5.1 (c) with further increase in the weight % of dopant into the structure results in the loss of the meso-porosity of the support frame work and this loss in the meso-porosity of the alumina is more prominent in the higher weight % (>1 wt%) of ceria doped catalyst as revealed by the

Figure 5.1 (d), this structure loss is due to the formation of the CeO_2 crystals that blocks the pores of the support and forms solid solution with the support thus increases the compactness of the support. This observation is in complete agreement with the XRD results that is with the increase in the dopant weight %, crystals formation takes and that in turn leads to the formation of the solid solution of ceria with alumina. These results also shows another interesting behavior regarding VO_x distribution that is with the increase in the ceria content into the alumina support the distribution of the VO_x decreases this can be firstly attributed to the collapse of the mesoporous structure of the support and secondly due to the increase in the acidity of the support with higher ceria content [63].

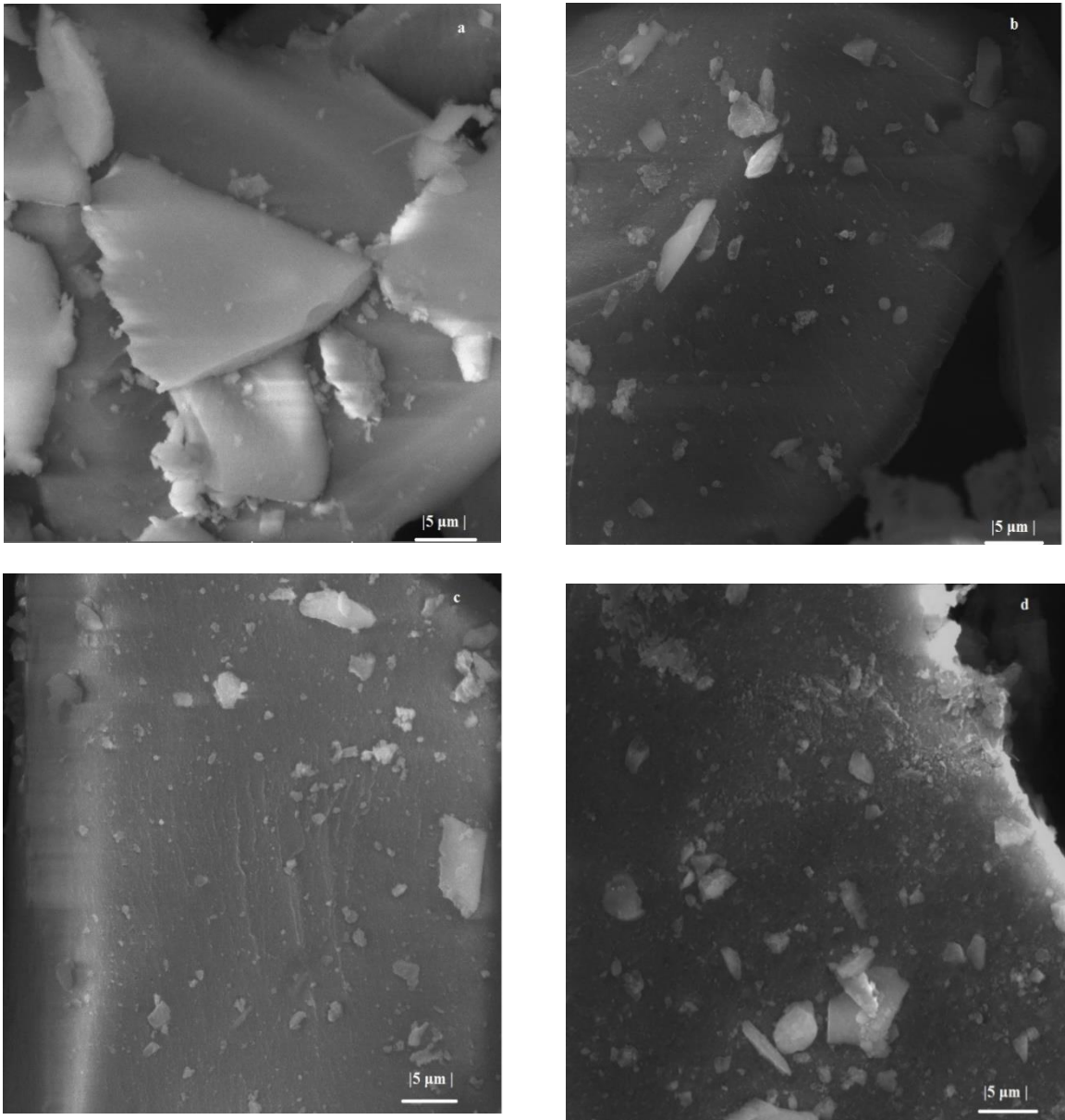


Figure 5.1. Secondary Electron images (SEI) of the (a) MAs (b) 0.2 Ce (c) 1.0 Ce (d) 5.0 Ce

5.1.2 X-ray diffraction (XRD) analysis results

Figure 5.2 represents typical XRD patterns of the MAs support, and VO_x/Ceria modified MAs catalyst samples. As it can be noted from Figure 5.2 (a) and (b) that both VO_x/MAs and MAs shows same diffraction pattern as that of pure MAs support, diffraction peaks that appears at around $2\theta = 37.0^\circ$, 45.5° and 67.0° are assigned to pure γ - Al₂O₃ according to JCPDS card 10-0425 [56]. The absence of VO_x peaks is related either to the formation of highly dispersed amorphous phase of VO_x or formation of very small crystals of VO_x which are undetectable by the XRD. These finding are in complete agreement with the already published work [8,62,64]. The 0.2 Ce catalyst (Figure 5.2 (c)) shows no XRD peaks for CeO₂ and it almost retain the MAs support structure with only little modification which is due to the presence of the amorphous CeO₂ phase. But as the dopant wt % is increased from 0.2 to 5 wt%, clear peaks appear that indicate the formation of crystalline CeO₂. While the MAs peaks intensities decrease and become the background in the XRD pattern due to presence of high intensity peaks of the dopant CeO₂ in the MAs matrix [53]. As the Ceria content in the catalyst is increased the peak intensities corresponding to ceria also becomes sharper and long, thus the spectrum appearing at 2θ of 28.5° , 33.0° , 47.2° , 56.1° , 58.5° , 76.5 and 79.0° are the diffraction lines given to the formation of the fluorite type of cubic crystals structure of CeO₂ (JCPDS 34-0394) [65]. Further, there is no evidence of the formation of the solid solution between VO_x and alumina because of the absence of AlV₃O₉ peaks which suggests no reaction between vanadium and the support.

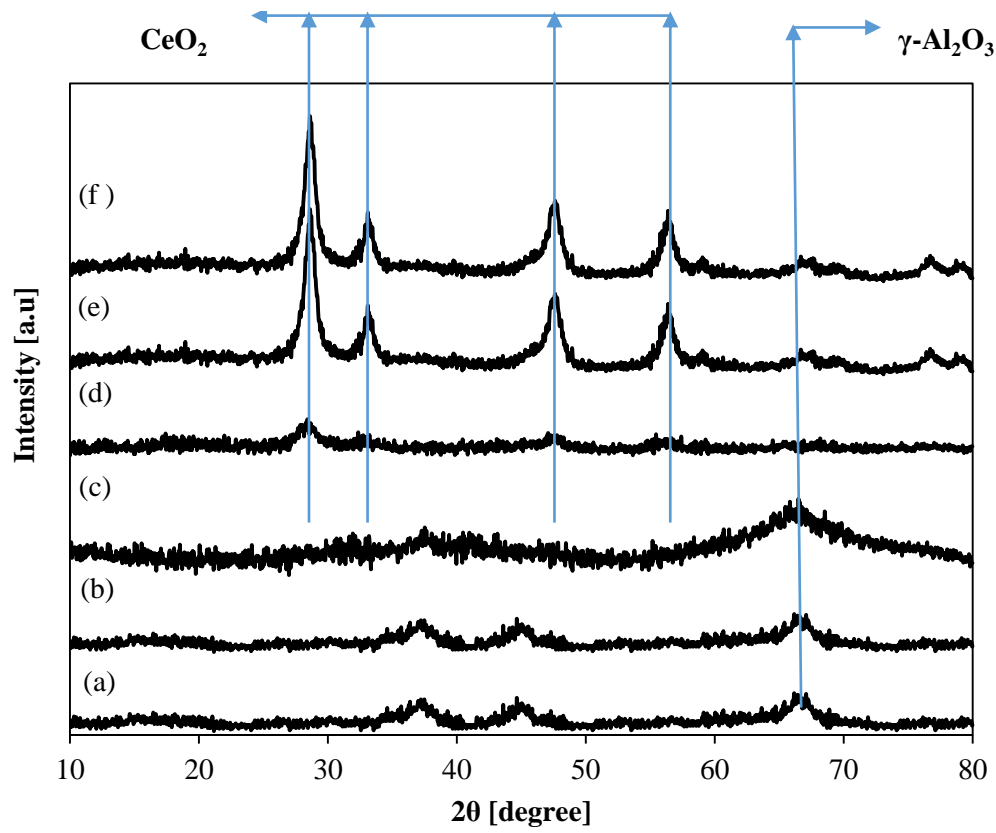


Figure 5.2. XRD spectra of (a) MAS (b) $\text{VO}_x/\gamma\text{-Al}_2\text{O}_3$ (c) 0.2 Ce (d) 1.0 Ce (e) 3.0 Ce (f) 5.0 Ce

5.1.3 Raman spectroscopy

Figure 5.3 represents the Raman spectra for the prepared catalyst in 100-1200 cm^{-1} range. MAs support shows no Raman spectra as it is expected due to ionic nature of the Al-O bond [66]. The appearance of the VO_x spectra depends on the vanadium loading and surface concentration of the VO_x species. Only a weak spectra appears at 1130 cm^{-1} for VO_x impregnated on the 0.2 Ce catalyst as shown by the Figure 5.3 and this transmittance is attributed to the highly dispersed monovanadate surface species having isolated tetrahedral structures. 3.0 Ce catalyst also exhibits similar Raman spectra but with the greater intensity of the peak at 1130 cm^{-1} . As the ceria content in the MAs framework is further increase to 5 wt%, then a secondary weak spectra at 950 cm^{-1} is also observed and it can be assigned to the V-O-V bond responsible for the crystalline V_2O_5 formation, Those sample shows the coexistence of the both polyvanadate and monovanadate surface species [37]. These results are in complete agreement with the XRD and TPR results that is with increase in ceria content the dispersion of the VO_x decreases which in turn promotes the formation of the crystalline phase of the vanadium oxide. Finally, CeO_2 shows Raman spectra at 460 cm^{-1} wavenumber which is more prominent in 3.0 Ce and 5.0 Ce catalyst samples and this band is the characteristic of the fluorite-structure CeO_2 , as also confirmed by the XRD results [67].

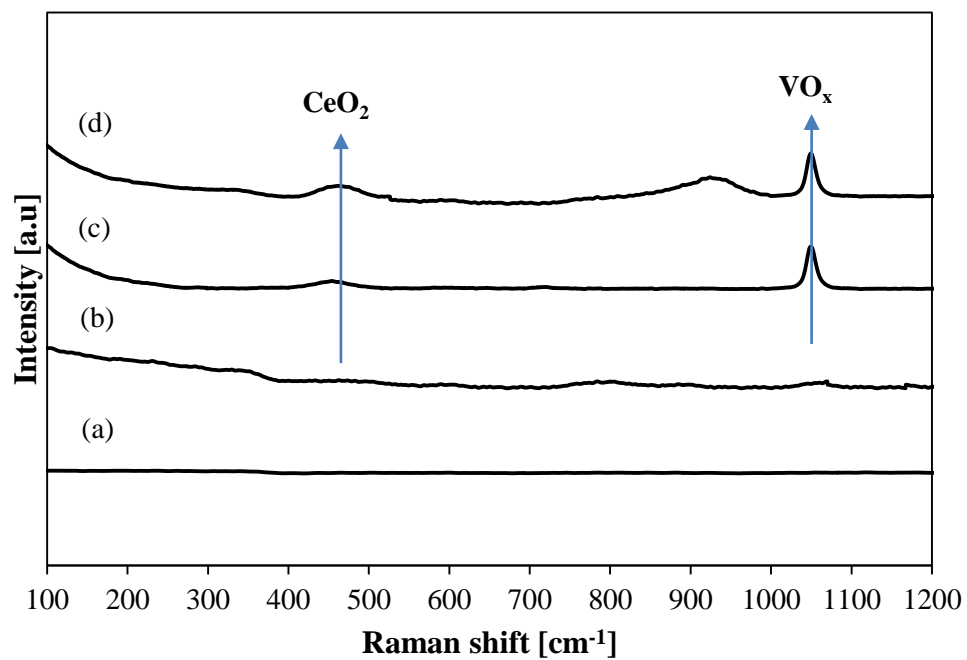


Figure 5.3. Raman spectra of the (a) MAO support, (b) 0.2 Ce, (c) 3.0 Ce, and (d) 5.0 Ce catalysts

5.1.4 FTIR spectroscopy

Figure 5.4 represents the FTIR spectra of the $\text{VO}_x/\text{CeO}_2\text{-MA}$ with different wt% of the ceria (0.2, 1, 3, and 5 wt%). All samples give broad spectral band between 3000-3800 cm^{-1} wavenumber and a weak band at 1650 cm^{-1} . These bands are assigned to the O-H stretching frequency of the adsorbed water and or due to surface hydroxyl group [68]. The FTIR peaks below 1100 cm^{-1} are attributed to Al-O and VO_x bonds stretching, both surface oxide species give the vibrations at almost the same wavenumber. Ce-O bonds vibration is reported in the range of 440-500 cm^{-1} [62,69]. Finally, the transmittance at 830 cm^{-1} is due to the vibration of the V-O-V bond bridge while absorption around 1100 cm^{-1} is assigned to V = O stretching frequency [70].

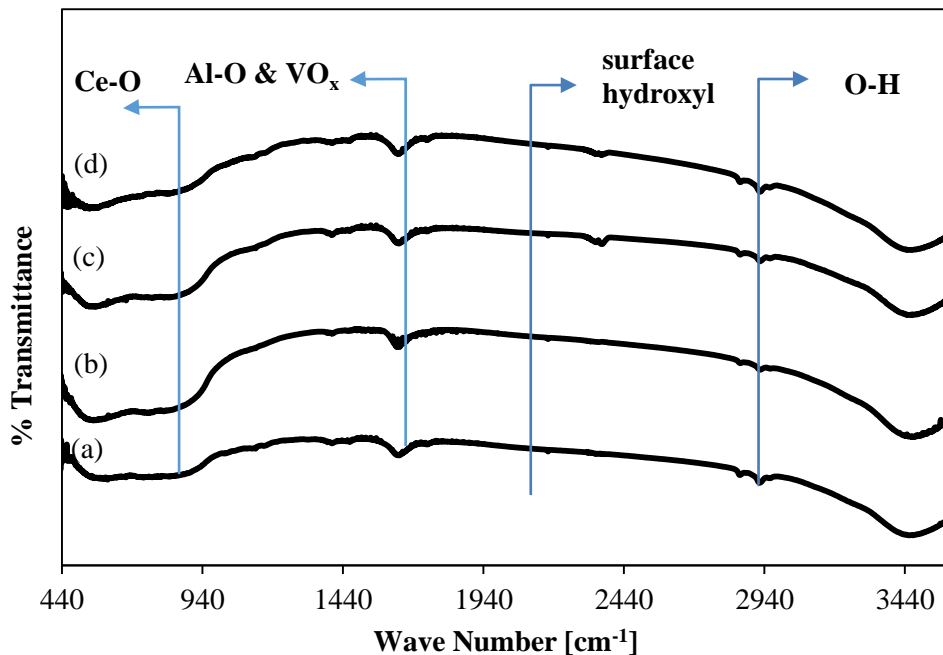


Figure 5.4. FTIR spectra of (a) 0.2 Ce (b) 1.0 Ce (c) 3.0 Ce (d) 5.0 Ce

5.1.5 Thermogravimetric analysis

The TGA curves for the synthesized catalysts in Figure 5.5 shows good thermal stability in the reaction temperature range of 350-650 °C. There is only one derivative weight loss peak for the all the sample, which appears at the range of 95-120 °C representing the evaporation of the adsorbed water from the pores of the catalysts and due the reduction of the surface nitrates species. If we compare the curves with the type of the catalyst, it is found that the catalyst having higher content of ceria (5.0 Ce) shows less weight loss and hence give higher thermal stability than the one with low ceria loading (0.2 Ce). In fact, these results are in full agreement with the literature that ceria acts to thermally stabilize the support [71].

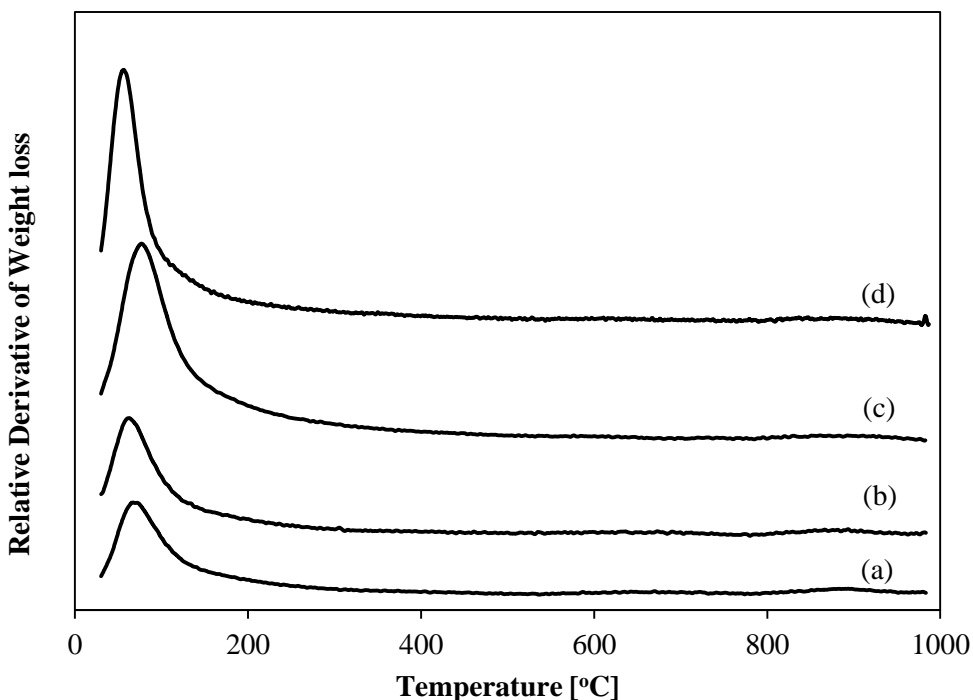


Figure 5.5. TGA Weight loss curves (a) 0.2 Ce (b) 1.0 Ce (c) 3.0 Ce (d) 5.0 Ce

5.1.6 Total acidity and metal support interaction (NH₃-TPD)

Temperature programmed desorption analysis is widely used to determine the metal support interaction, total acidity and strength of the acidic sites. These are the key properties of the ODH catalyst that determine the selectivity of desired products in anaerobic ODH reactions. In fact, a close correlation can be developed between the acidic nature of the VO_x supported catalysts and their catalytic activity toward the formation of the selective products [72,73].

The small molecular size and strong basicity of NH₃ enables it to investigate the acidity at the broad range of temperature for the catalysts having pores dimension $\geq 4 \text{ \AA}$. The mechanism of the NH₃-TPD analysis is based on the sorption strength to determine the total acidity, that is the sum of the Brønsted and Lewis acidic sites, thus this technique is unable to differentiate between these two acidic sites [74]. In the typical analysis, NH₃ is first adsorbed at 120 °C followed by desorption between 120 °C to 850 °C at the heating rate of 10 °C/min. while the effluent gas concentration is monitored by the thermal conductivity detector (TCD).

Figure 5.6 shows the TPD profile for the prepared VO_x/Ce-MAs catalysts having different wt% of the dopant ceria. The total acidity of each sample was determined by finding the total area under the curve of TCD signal vs temperature. The total acidity along with the maximum desorption temperature is given in the Table 5.1. All the samples showed a broad initial NH₃ desorption peak with the center at $\sim 195 \text{ °C}$, while the higher temperature desorption peak was observed at $\sim 544 \text{ °C}$. The low temperature desorption peaks were assigned to the NH₃ desorption from weak and moderate acidic sites, while the

high temperature desorption corresponds to desorption of chemisorbed NH_3 from strong acidic sites.

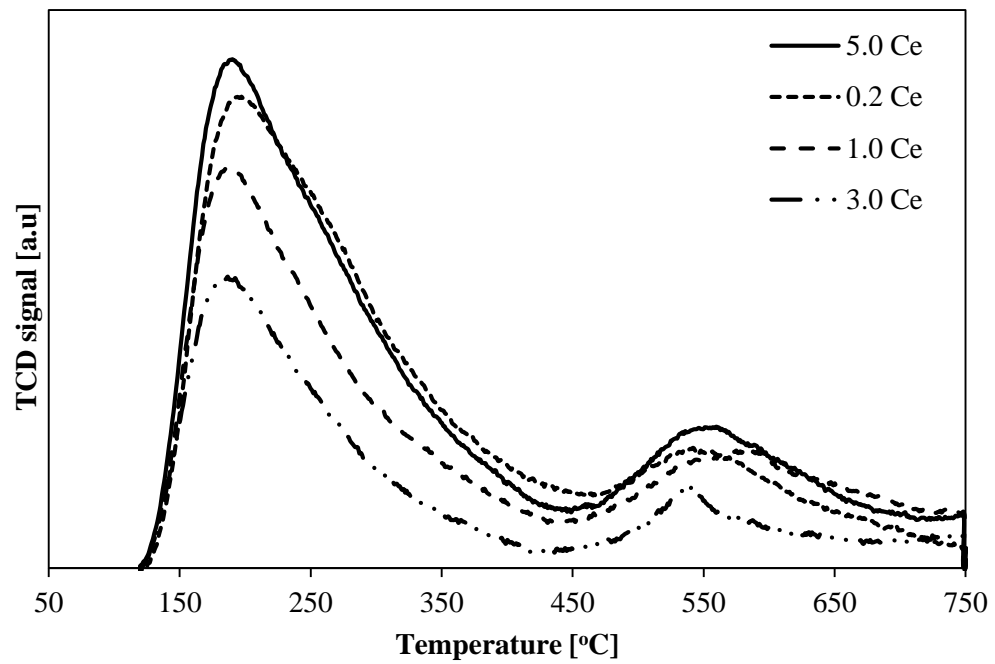


Figure 5.6. NH_3 -TPD analysis: TCD signal vs Temperature for 0.2 Ce, 1.0 Ce, 3.0 Ce and 5.0 Ce catalysts

The combined effect of both the dopant (Cerium) and active metal oxide (VO_x) in the sample was to reduce the total acidity of the support, while the sample with more wt % of the dopant shows higher acidity than the one having lower ceria content. It shows a good interaction between the support and the metal oxide. It is reported by [75,76] that ceria modified catalyst would increase the acidity by creating new acidic sites on the surface of the support which gives rise to increase in the acidity with the amount of the ceria. Secondly it was also reported by [8] that presence of VO_x can increase the concentration of Brønsted acidic sites as compared with the concentration of Lewis acidic site (related with $\gamma\text{-Al}_2\text{O}_3$). So higher the ceria content, the greater is the promotion of the Brønsted sites and the greater will be the acidity of the catalyst.

Table 5.1. Total acidity and maximum reduction temperature

Catalyst	Total acidity [cm^3/g]	Max T1 [$^{\circ}\text{C}$]	Max T2 [$^{\circ}\text{C}$]
0.2 Ce	9.96	200	549.5
1.0 Ce	10.45	196.5	547
3.0 Ce	12.45	193.2	543
5.0 Ce	13.1	191.7	542.2

The NH₃-TPD experimental data was fitted into the desorption kinetic model, in order to determine the activation for NH₃ desorption (E_{des}) and the intrinsic kinetic parameter (k_{des0}). Evaluation of these parameters are very necessary to relate them with the metal support interaction. Following assumptions were considered prior to the estimation of the kinetic parameters [75,77];

- I. The uniform NH₃ concentration over the homogeneous catalyst surface.
- II. Ammonia desorption is governed by the first order rate law having constant rate of desorption, independent of the surface coverage of the catalyst.
- III. Readsorption of the desorbed NH₃ is almost negligible.
- IV. A linear increase in the temperature of the catalyst bed with respect to the time.

The NH₃-TPD experiments were conducted in such a way to fulfil the above mentioned assumptions. By performing the mass balance on the adsorbate and following the procedure mentioned in [60,78], frequency factor and ammonia desorption is given by;

$$K_d = k_{des0} \exp\left(\frac{-E_{des}}{R T}\right) \quad (5.1)$$

$$r_{des} = -V_m \left(\frac{d\theta_{des}}{dt}\right) = k_{des0} \theta_{des} \exp\left(\frac{-E_{des}}{R} \left(\frac{1}{T} - \frac{1}{T_n}\right)\right) \quad (5.2)$$

Where, θ_{des} is the surface coverage, K_d is the desorption constant, while k_{des0} , E_{des} , and T_n are the pre-exponential factor, activation energy for desorption, and centering temperature respectively. For the constant ramping rate (β), the following linear correlation can be developed;

$$T = T_n + \beta t \quad (5.3)$$

Differentiating w.r.t time (t)

$$\frac{dT}{dt} = \beta \quad (5.4)$$

Chain rule can be used to correlate the surface coverage (θ_{des}) with the ramping rate (β), as given below;

$$\left(\frac{d\theta_{des}}{dt}\right) = \left(\frac{d\theta_{des}}{dT}\right) \left(\frac{dT}{dt}\right) = \beta \left(\frac{d\theta_{des}}{dT}\right) \quad (5.5)$$

By using Equations 5.2 and 5.5;

$$\left(\frac{d\theta_{des}}{dt}\right) = -\frac{k_{des0}}{V_m \beta} \theta_{des} \exp\left(\frac{-E_{des}}{R} \left(\frac{1}{T} - \frac{1}{T_n}\right)\right) \quad (5.6)$$

The surface coverage can also be given by;

$$\theta_{des} = 1 - \frac{V_{des}}{V_m} \quad (5.7)$$

Equations 5.6 and 5.7 gives rise to;

$$\left(\frac{dV_{des}}{dT}\right) = \frac{k_{des0}}{\beta} \left(1 - \frac{V_{des}}{V_m}\right) \exp\left(\frac{-E_{des}}{R} \left(\frac{1}{T} - \frac{1}{T_n}\right)\right) \quad (5.8)$$

Where V_{des} is the total volume of the NH_3 desorbed (ml/g cat).

Mathematica NonlinearModelFit built-in function was used to fit the experimental data into the desorption model, governed by Equation 5.8. The amount of the catalyst (0.1 g) and ramping rate ($\beta = 10 \text{ }^\circ\text{C}/\text{min}$) was kept constant in each TPD analysis. The desorption parameters were estimated with 95% Confidence interval and their estimated values are given in the Table 5.2.

Table 5.2. Estimated Desorption parameters at $\beta = 10$ °C/min

Samples	k_{desO} (cm^3/min)	E_{des} (kJ/mol)	R^2	AIC	V_{des} (ml/g cat)
0.2 Ce	$1.67 \times 10^{-4} \pm 0.0022$	1.94 ± 0.18	0.99	-45379	9.96
1.0 Ce	$2.65 \times 10^{-4} \pm 0.0038$	1.75 ± 0.19	0.99	-41149	10.45
3.0 Ce	$2.10 \times 10^{-4} \pm 0.0025$	1.50 ± 0.15	0.99	-44664	12.45
5.0 Ce	$3.50 \times 10^{-4} \pm 0.0046$	1.45 ± 0.18	0.99	-38882	13.1

A close match between the experimental data and the model prediction is due to higher value of correlation coefficient ($R^2 > 0.99$), large degree of freedom ($F \sim 5572$) and a high confidence interval (95%). Secondly the good quality of the nonlinear regression model fitting is also revealed by the large negative value of Akaike Information Criterion (AIC).

The lower desorption energies for all prepared catalysts given in Table 5.2 as compared with the $\text{VO}_x/\gamma\text{-Al}_2\text{O}_3$ reported in the literature [62] indicates lower metal support interactions. So, ceria doped catalyst generally will be more active for the ODH of n-Butane as compared with the pure support. The catalysts with more ceria content require less energy to desorb NH_3 from its surface, showing more availability of the lattice oxygen which will make it more active but at the same time it will be less selective towards the ODH reactions because of the easy availability of the lattice oxygen. While the catalyst having less ceria wt% need more energy to desorb the NH_3 implying more metal support interaction than the one with higher ceria content, this in turn will make it less active but more selective for the ODH reaction. Similar results have been reported by the [79] for

the Ni/Al₂O₃ catalysts, in which the catalyst with less impregnation of active metal oxide showed higher activation energy that leads to strong metal support interaction.

These TPD kinetic modeling results are in complete agreement with the TPR results, which shows higher activity for the catalyst having more ceria wt% that will cause more H₂ consumption. XRD characterization results also re-confirmed these NH₃-TPD results by showing more intense peaks for CeO₂ at higher dopant loading. According to the literature [71] the more the ceria in the catalyst the more will be the lattice oxygen available.

5.1.7 Temperature programmed reduction (TPR)

The gas phase oxygen free ODH mainly rely on the ease of the removal of the selective lattice oxygen, the reducibility of the catalyst and the nature of the oxide phases present on the surface of the catalyst. In this regard, H₂-TPR studies can easily demonstrate these important catalytic properties. The nature of the oxide phase formed on the surface of the catalyst depends on several factors such as: catalyst synthesis method, type of the active metal oxide, nature of the support used, and calcination temperature implied during catalyst preparation.

The TPR profiles of the VO_x/Ce-MAs catalysts with different ceria content are shown in the Figure 5.7. The reduction profile of the all samples shows a large reduction peak with the maximum reduction temperature ranging from 429-465 °C. The reduction in this temperature range is attributed to the reduction of amorphous monomeric or polymeric VO_x phase having oxidation state between V⁺⁵ and V⁺⁴ according to the literature [80,81]

Further, the surface reduction of the Ceria oxide phase also take place in this temperature range and these peaks are overlapped by the major VO_x reduction peak [82].

The second small high temperature peak displayed at 800 °C is assigned for the bulk reduction of CeO_2 phase, this high temperature reduction implies strong interaction with the support material [83,84], it is noted as the CeO_2 content in the catalyst increases so thus the peak intensity of this high temperature reduction also increases, this peak actually hide in the background for the catalyst having lower wt% of ceria (< 1 wt%), due to the presence of the main peak of the VO_x . These results are in complete agreement with the XRD results which also shows increase in the intensity of the CeO_2 peaks with its wt% in the matrix. A similar trend is also observed in XRD that gives no peaks for the catalysts containing 1% or less ceria content due to formation of the amorphous phase of CeO_2 .

There is another second important finding that is lower temperature reduction peak shifts slightly toward the right side as the amount of the ceria in the catalyst is increase. Confirming the formation of the more stable monomeric surface species which are believed to reduce at higher temperature as compared with the polymeric VO_x phase [82]. These results also confirmed the TGA analysis that is when CeO_2 is doped in the sample it tends to increase the thermal stability of the catalyst [84].

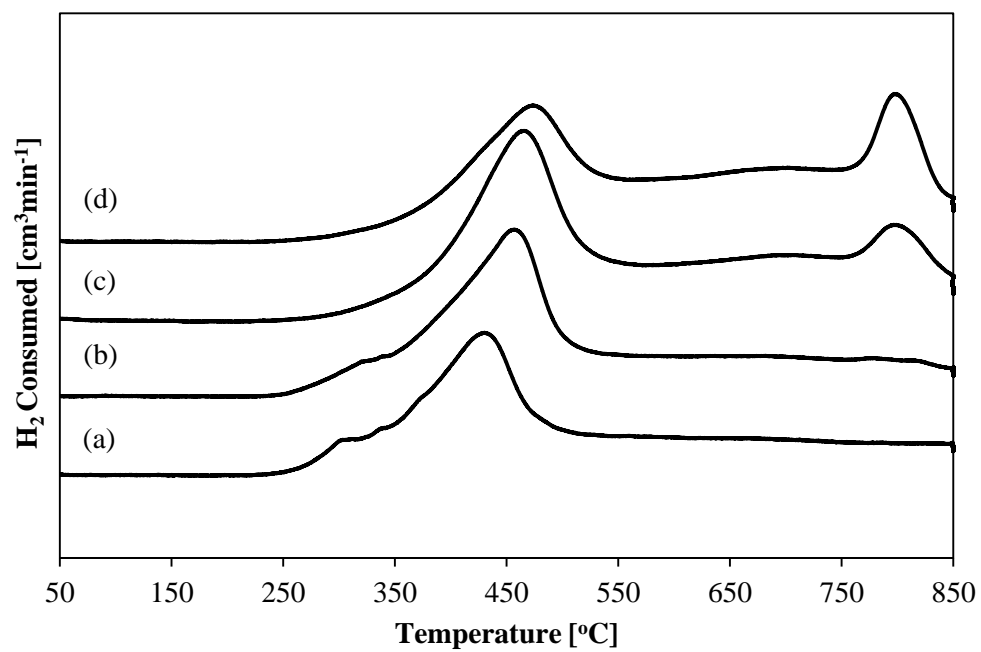


Figure 5.7. TPR profile of (a) 0.2 Ce (b) 1.0 Ce (c) 3.0 Ce (d) 5.0 Ce

The amount of H₂ consumed can be find out by calculating the area under TPR curve. Typical average value for H₂ uptake is shown in the Figure 5.8. As the VO_x (~4.5 wt %) content on all catalysts is same so they gives almost comparable consumption of H₂ despite of the fact that they contain different amount of dopant. This is due to the stable nature of the ceria which tend to increase the thermal stability of the catalyst. In fact, at higher ceria content (> 1 wt%) the samples tend to give more crystallize CeO₂ phase formation and reduction of this crystalline phase increases the peak intensity of the higher temperature reduction which in turn increase the H₂ consumption.

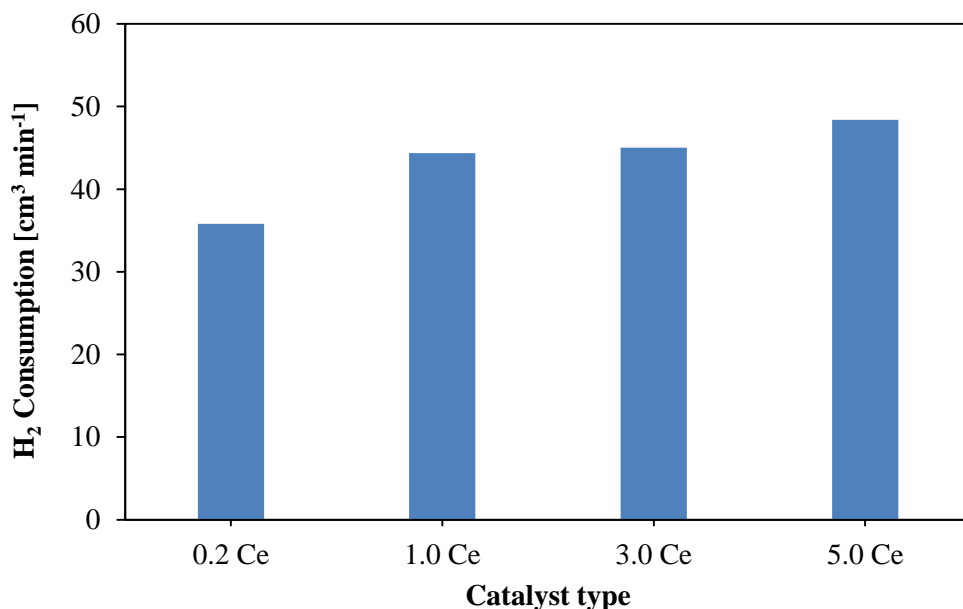


Figure 5.8. H₂ consumption for 0.2 Ce, 1.0 Ce, 3.0 Ce, and 5.0 Ce catalysts

Although, the H₂ consumption is large for the high ceria containing catalysts but still low ceria containing catalysts (<1 wt%) is believed to work better than their counterpart due to good dispersion of VO_x and secondly ceria is reported to promote complete oxidation reaction. That's why 0.2% ceria doped VO_x/MAs catalyst is selected. In order to check the reducibility and reoxidation, the catalyst is subjected to repeated TPR/TPO cycles as shown in the Figure 5.9. After the first cycle the peaks are slightly shifted toward higher temperature and H₂ consumption also decreases slightly but soon after the second cycle the H₂ consumption as well as the peak position almost remain the same.

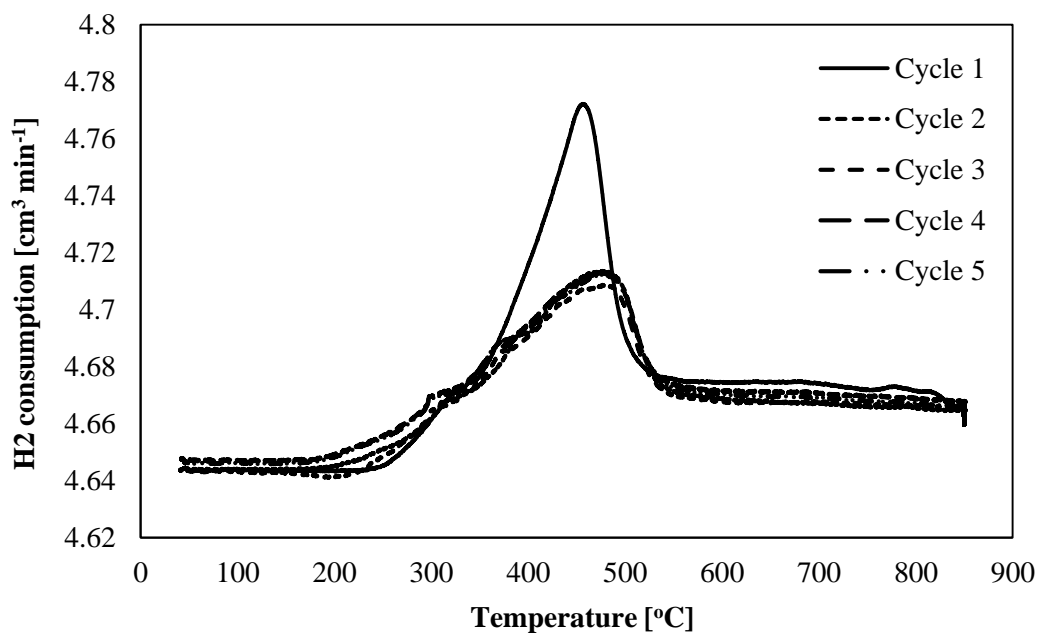
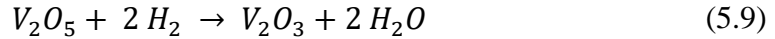


Figure 5.9. TPR/TPO cycles of 0.2 Ce catalyst

The reduction at low temperature with higher uptake of H₂ is due to the reduction of the nitrate species present on the fresh catalyst and soon after the first cycle of TPR these reducible nitrates are removed from the catalyst so finally not only the H₂ consumption become constant but also the reduction temperature remain the same for the next cycles. These repeated TPR/TPO not only show the catalyst stability during repeated oxidation and reduction cycles but also tell us that there is no thermal sintering and phase transformation take place during the redox cycle.

The actual ODH reaction can easily be explained by TPR/TPO analysis because of the resemblance of the reduction of the catalyst in the real reaction with that of H₂-TPR as shown by the Equation 5.9.

Reduction of the catalyst by H₂-TPR



TPR data can be used to find out the percentage reduction of vanadium oxide for each sample. The degree of reduction can be defined as the ratio of the amount of vanadium oxide reduced during TPR cycle to the total vanadium oxide present on that sample. The fractional amount of reducible vanadium can be calculated by using Equation 5.10

$$F_v = \frac{MW_v \times V_{H_2}}{v \times V_g \times W_o} \quad (5.10)$$

Where, MW_v is the molecular mass of vanadium (g/mol), V_{H_2} is the volume of the hydrogen consumed per cycle (cm^3 at STP), v is the stoichiometric coefficient of H_2 given in Equation 5.9, V_g is the molar volume of the hydrogen (cm^3/mol at STP) and W_o is the total amount of the reducible vanadium on the catalyst taken for TPR analysis (g). If only V_2O_5 is supposed to be present on the catalyst surface as shown by Equation 5.9, then the F_v for the 1st, 2nd and 3rd cycles for 0.2% ceria loaded catalyst is 82.75%, 78.94% and 77.125% respectively and then remain constant at almost 77 % for following cycles as shown by Figure 5.10. The % reduction of vanadium can be used to calculate the nature of the oxide phase present on the surface of the catalyst known as the average oxidation state. For the selected catalyst the value of the average oxidation state is 3.42 or can be written as $V_2O_{3.42}$ and most probably it will V_2O_3 oxide phase.

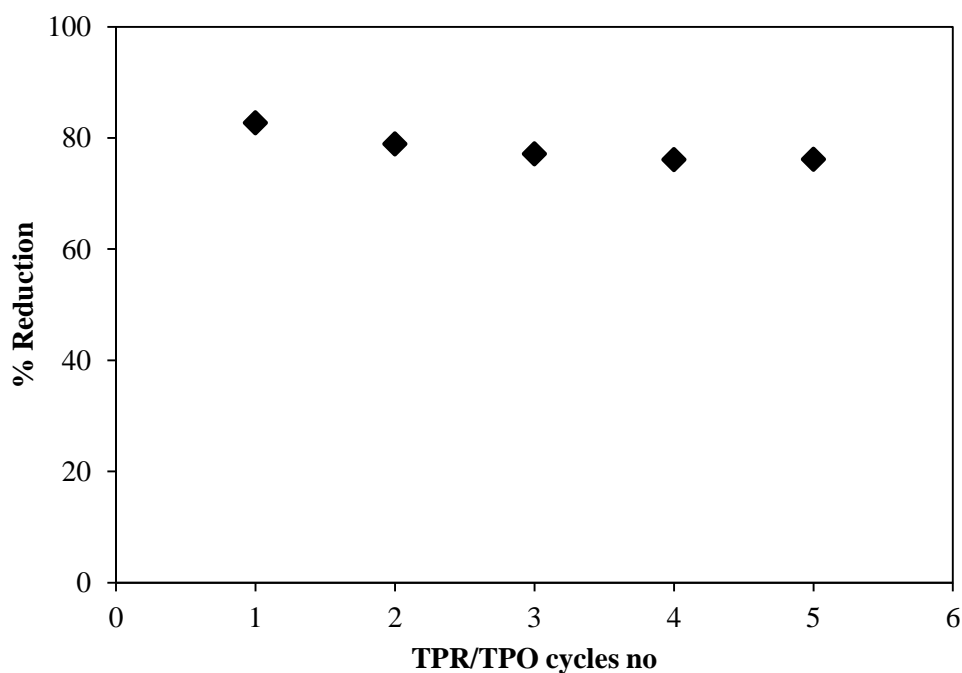


Figure 5.10. The % reduction of vanadium

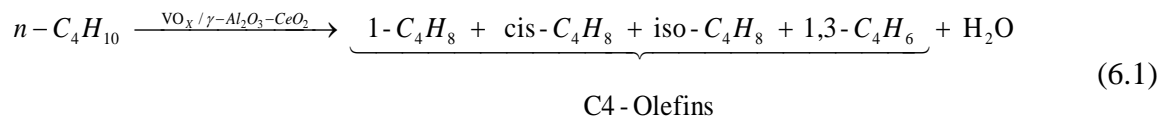
CHAPTER 6

ODH of n-BUTANE AND REACTION KINETICS

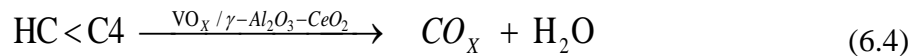
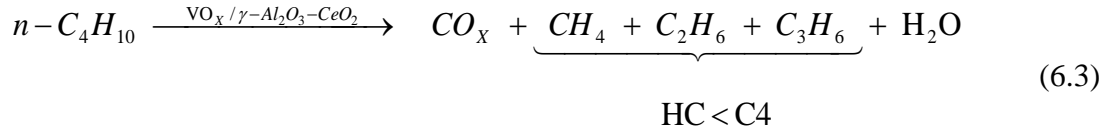
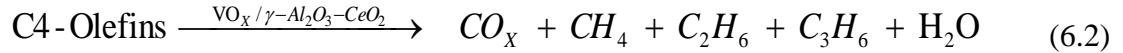
6.1 Catalyst Evaluation in Fluidized bed reactor

The anaerobic ODH experiments over the synthesized catalysts were conducted under fluidized bed reaction conditions. The reaction temperature range was set between 450 to 600 °C (based on TPR profile) while the contact time was varied from 5 to 25 sec. The temperature of the catalyst was gradually increase from room temperature to the reaction temperature under argon flushing and after each ODH experiment the reduced catalyst was regenerated with the supply of air at 575 °C for 10 min and after this regeneration, the catalyst was flushed with argon for 15 min. The feed to the reactor was pure n-butane (99.97% n-butane). All ODH experiments were conducted at atmospheric pressure (14.67 psi) and constant impeller speed of 4000 rpm, and at the same feed to catalyst ratio of 1 ml of n-butane/1.0 g. All possible reactions during the ODH based on the online GC analysis are as follows:

Desired reactions:



Undesired reactions:



The ultimate goal will be to maximize the yield of the desired product first by selecting the selective catalyst and later by finding the suitable reactions conditions that favors the formation of C4-olefins. The ODH reactions were preceded by several thermal blank runs to determine the possible contribution of the thermal cracking reactions on the catalytic ODH reactions. These thermal runs were conducted at 10 sec reaction time and at the same temperature range (450 – 600 °C) as selected for ODH experiments. Figure 6.1 reports an increasing trend of n-butane conversion as a function of temperature under anaerobic condition. It can be noted from Figure 6.1 that the n-butane displayed low conversion values ranging from 1.2 to 3.50 %, showing limited contribution due the homogenous gas phase reactions. Thus based on these blank runs, the conversion observed in the ODH reactions can be purely assigned to the activity of the VO_x/Ce-MAs catalyst.

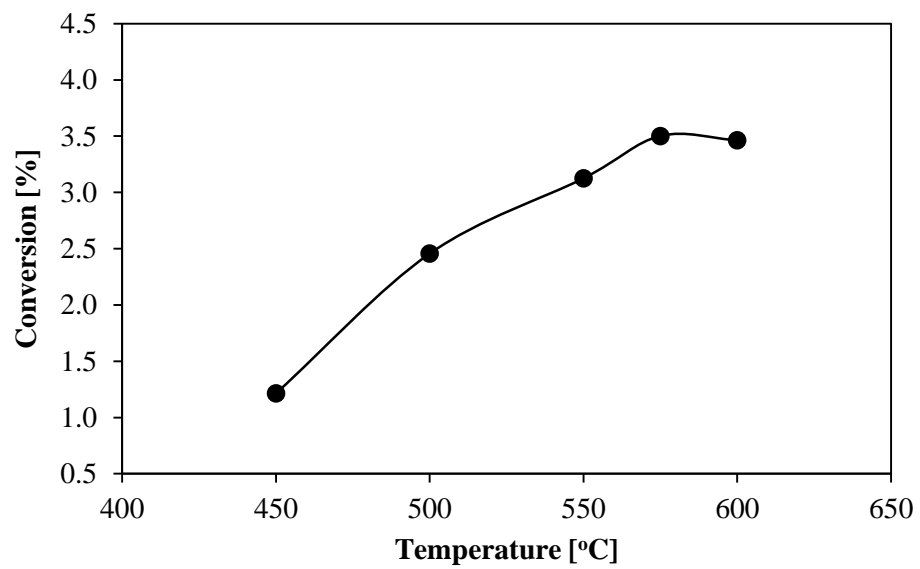


[Figure 6.1 Blank run (2 ml butane injection, t=10 sec)]

The typical product distribution for the ODH of n-butane over the two extreme condition of the temperature i.e. 450 and 600 °C on 0.2 Ce catalyst is shown in Figure 6.2. One can see that the product ranges from CH₄ to C₄H₈ isomers. Figure 6.2 represents the typical ODH reaction behavior for n-butane, at low temperature the selectivity of the C₄-olefins is high but at the expense of the conversion, indicating that low temperature favors the desired reaction represented by Equation 6.1. On the other hand, at higher temperature the catalyst tend to lose the lattice oxygen easily which give rise to higher conversion but the yield of the desired product decreases sharply. The mole fraction of the CO_x as well as the degradation product also increases at elevated temperature which means that the catalyst tend to favor the undesired reactions (complete combustion + cracking reaction) represented by the Equations 6.2, 6.3, and 6.4. So a general trend mentioned by [15] is that at low conversion higher selectivity of the desired product and vice versa.

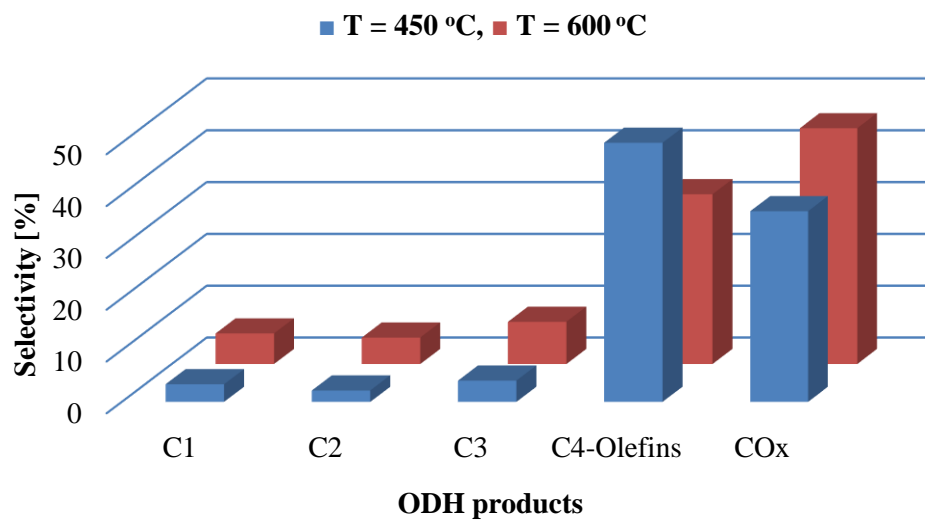


Figure 6.2. The typical product distribution for the ODH of n-butane over the two extreme condition of the temperature (450 & 600 °C) on 0.2 Ce catalyst (t = 10 s, w = 1 g, feed = 1 ml)

The effect of the ceria loading on the catalytic behavior of $\text{VO}_x/\gamma\text{-Al}_2\text{O}_3$ for the gas phase O_2 free ODH is shown by the Figure 6.3. These experiments were conducted at 500 °C temperature, 10 sec reaction time, 4000 rpm impeller speed and the Catalyst/feed ratio was set at 0.5. The results shows that the 0.2 Ce catalyst gives highest C4-olefins selectivity but lower conversion, while the 5.0 Ce catalyst gives highest conversion and selectivity for the CO_x . Thus if yield (selectivity x conversion) is the selected as the criterion for the selection of best catalyst then 0.2 Ce Catalyst works best among the others. These results can be explained based on the TPD and TPR characterization results that those catalysts having higher ceria content have more reducible surface species represented by the more H_2 uptake, while at the same time have lower desorption energy so have less metal support interaction which actually make them more reactive that why give higher conversion but due to presence of more easily reducible CeO_2 phase present on their surfaces as revealed by the more intense XRD peaks, leads toward the complete combustion.

Secondly, higher ceria containing catalysts have more acidity and according to the literature [25,26,63] it favors the cracking reaction and these degraded fraction can further react with the lattice oxygen of the catalyst and give rise to CO_x formation. On the other hand, catalyst containing lesser ceria have more metal support interactions indicated by the less H_2 consumption, thus will show more compactness for the lattice oxygen [1,8,37] and will have small conversion but at the same time due to small acidity and more selective surface oxides species will have less degradation products and more C4-olefins production [23]. On the basis of these findings 0.2 Ce catalyst will be considered for further evaluation.

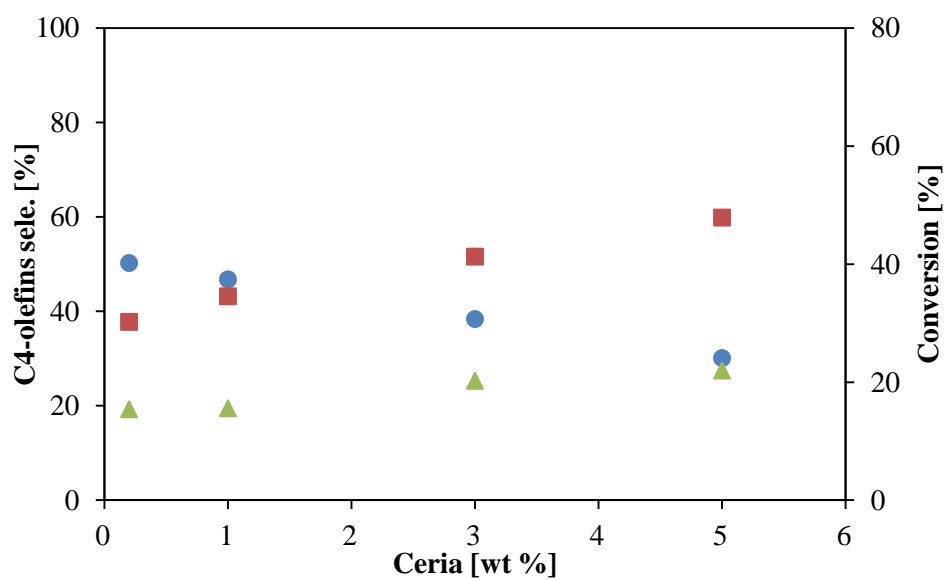


Figure 6.3. Effect of butane conversion, C4-olefins selectivity and CO_x selectivity on 0.2 Ce, 1.0 Ce, 3.0 Ce and 5.0 Ce catalysts, ● C4-olefins selectivity, ■ CO_x selectivity, ▲ butane conversion (t = 10 s, w = 1 g, feed = 1 ml, T = 500 °C)

The effect of the reaction temperature on the C4-olefins selectivity at different reaction time is shown by the Figure 6.4. The graph represents typical ODH behavior reported by [22–24,27] that at high temperature there will be more C-H bond activation that will leads toward higher conversion but at the same time there will be more cracking and complete combustion of the feed and the C4-olefins [1] that is the higher the temperature the more susceptible the feed and the C4-olefins will be towards degradation and ultimately CO_x formation as shown by simple reaction mechanism [40].

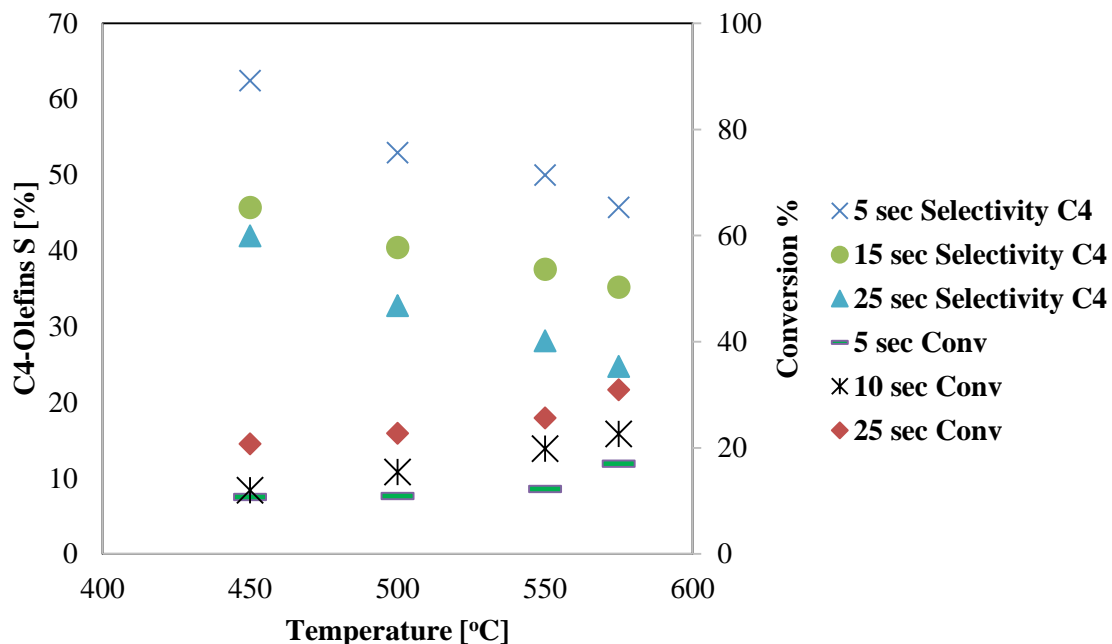


Figure 6.4. Effect of temperature on product selectivity, 0.2 Ce Catalyst (t = 10 , 15, 25 s, w = 1 g, feed = 1 ml)

The catalyst is further evaluated by considering the effect of the reaction time on the C4-Olefins selectivity as shown by Figure 6.5 showing similar trend as previously represented by the temperature that is the more the time the reactant takes in contact with the catalyst more will be the production of CO_x and cracking fractions as also reported by the many researcher [11,30].

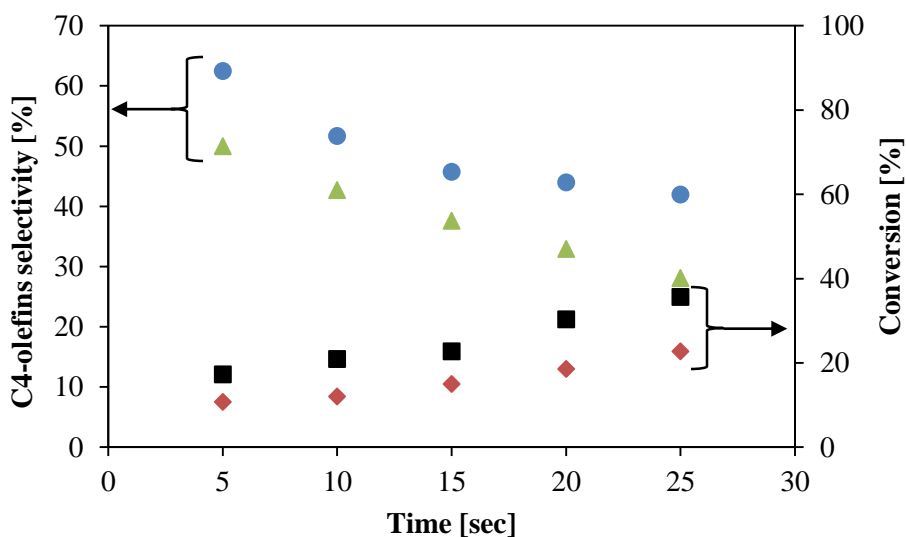


Figure 6.5. Effect of contact time on C4-olefins selectivity over 0.2 Ce catalyst, ● C4-alkenes sele. at 450 °C, ▲ C4-alkenes sele. at 550 °C, ■ n-butane conv. at 550 °C, ◆ n-butane conv. at 450 °C (feed = 1 ml, w = 1 g)

As expected and mentioned in the literature that CO_x will almost follow an opposite trend when compared with the C4-olefins selectivity. That is high temperature and more contact time will lead more CO_x mole fraction in the final product. This is because of the 1) direction complete combustion of n-butane, 2) C4-olefins further oxidation to CO_x and 3) cracked products activation by the lattice oxygen to yield CO_x .

Figure 6.6 reports four successive n-butane injection over four repeated oxidation reduction cycles at the same contact time (10 s) and reaction temperature (450 °C) and after each n-butane ODH run, the reduced catalyst was re-oxidized by air at 575 °C. The stable n-butane conversion and C4-olefins selectivity can be seen in Figure 6.6, confirming the stable nature of the ODH catalyst. These results are in complete agreement with the repeated TPR/TPO characterization results.

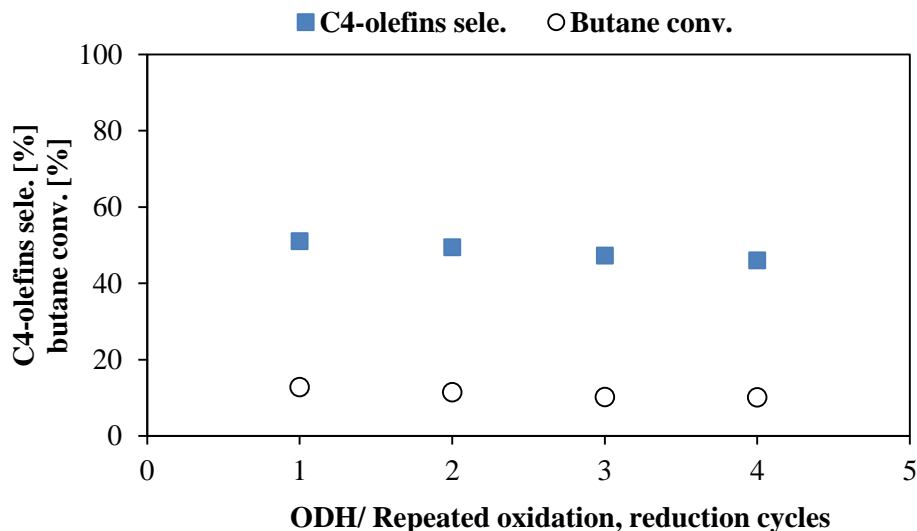


Figure 6.6. Butane conversion and C4-olefins selectivity over 0.2 Ce catalyst in consecutive ODH runs with catalyst re-oxidation (T = 450 °C, t = 10 s, w = 1 g, feed = 1 ml)

Figure 6.7 shows very interesting behavior when the successive butane injection is carried out without catalyst regeneration for the constant temperature and contact time. So with each successive injection the selectivity of C4-olefins increases while that of CO_x decreases as reported by many scientists [16,30]. This is due the presence of the nonselective surface oxide phase of both VO_x (mainly V₂O₅) and Cerium oxide having +4 activation state but as soon as this nonselective species are knock out then the catalyst shows higher affinity for C4-olefins production. The CO_x shows just the opposite behavior. While the conversion also decreases with each injection due to reduction of the lattice oxygen and that on the reduced catalyst requires higher energy.

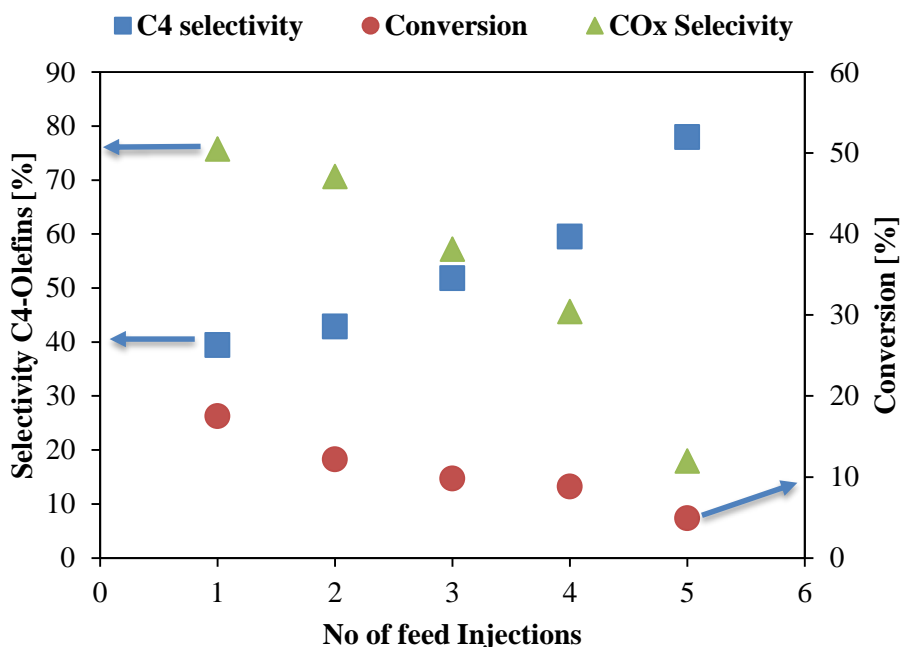


Figure 6.7. Effect of successive injection, T=500°C, t=5sec, 0.2% Ceria doped cat, feed/cat=0.5

Following are the key findings of this chapter:

1. Very little contribution from the thermal degradation and gas phase reaction to the ODH of n-butane was noticed.
2. 0.2 Ce catalyst gives more selective behavior toward the ODH of n-butane compared with the higher ceria containing catalysts, mainly because of its lower acidity and more metal support interaction.
3. Low reaction temperature and small contact time favor the yield of the C4-olefins.
4. Metal loading have almost no effect on the selectivity of the product, but the conversion shows increasing trend with the catalyst to feed ratio
5. The repeated oxidation/reduction experiments show that the catalytic results can easily be regenerated with less than 3% standard error.
6. Reduced catalyst works better than the fresh catalyst due to more packing of the lattice oxygen in the spent catalyst.

6.2 Kinetic Model formulation

This section reports kinetic model formation for ODH of butane in fluidized-bed reactor in anaerobic condition where the experimental data is fitted by LH mechanism that take into the account of catalyst reduction term as well. The incentive of using CREC Riser Simulator are: first isothermal reaction conditions are possible and secondly almost no mass transfer limitations due to high fluidization and finally presence of online facility for the re-oxidation of the spent catalyst enable its practical implementation at the industrial level. The successful fitting of MKV is reported by [42] for the gas phase oxygen free ODH of propane to propylene using $\text{VO}_x/\gamma\text{-Al}_2\text{O}_3$ catalyst using fluidizable bed batch reactor.

The anaerobic ODH reactions of butane over the 0.2 ceria modified VO_x/MAs were conducted at four different temperature (400, 500, 550, and 575 °C) and at five different residence time (5, 10, 15, 20, and 25 sec), the remaining process variables were kept constant at 4000 rpm, feed/catalyst = 0.5, pressure = 1 atm. Under such anaerobic conditions the reaction proceeds via the reduction of the catalyst. That's why catalyst reducibility was incorporated in the rate of reaction as mentioned by [8,42] as an exponential decay function given by Equation 6.5:

$$D = \exp[-\lambda(X_{C_4H_8})] \quad (6.5)$$

Where D is the catalyst degree of oxidation, λ is constant, and $X_{C_4H_8}$ is the butane conversion.

The reaction pathways as given by [41] is given below:

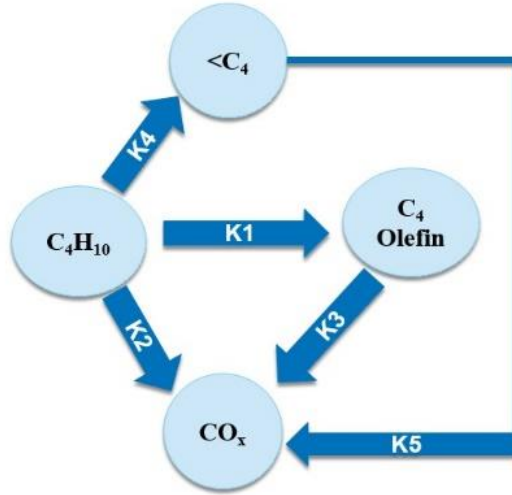


Figure 6.8. Parallel, series reaction network

The ODH experiments give lower mole fraction (<10%) for the degradation products (HC<C4), so HC<C4 reactions are not considered in the kinetic modeling. The differential rate equations based on Langmuir-Hinshelwood mechanism obtained after simple mathematical manipulation give the following three equations, where Equation 6.6 accounts for the total consumption of butane, Equation 6.7 represents the net rate of C4-olefins production while Equation 6.8 is attributed to the production of CO_x, the detailed formulation can be seen in the [8,41] articles.

$$\frac{d\theta_{C_4H_{10}}}{dt} = -\frac{Wt_{cat}}{V_R} \left(\frac{MW_{C_4H_{10}} V_R}{Wt_{HC}} \right) \times \frac{(k_1 + k_2) AK_{C_4H_{10}} y_{C_4H_{10}}}{Q} \times D \quad (6.6)$$

$$\frac{d\theta_{C_4H_8}}{dt} = \frac{Wt_{cat}}{V_R} \left(\frac{MW_{C_4H_8} V_R}{Wt_{HC}} \right) \times \frac{k_1 AK_{C_4H_{10}} y_{C_4H_{10}} + k_2 BK_{C_4H_8} y_{C_4H_8}}{Q} \times D \quad (6.7)$$

$$\frac{d\theta_{CO_x}}{dt} = \frac{Wt_{cat}}{V_R} \left(\frac{MW_{CO_x} V_R}{Wt_{HC}} \right) \times \frac{k_2 AK_{C_4H_{10}} y_{C_4H_{10}} + k_3 BK_{C_4H_8} y_{C_4H_8}}{Q} \times D \quad (6.8)$$

Where Q is given by:

$$Q = \left(1 + AK_{C_4H_{10}} y_{C_4H_{10}} + k_3 BK_{C_4H_8} y_{C_4H_8} \right) \quad (6.9)$$

Temperature dependency of the rate constant and adsorption constant is given by the Arrhenius equation:

$$k_i = k_i^o \exp \left[\frac{-E_i}{R} \left(\frac{1}{T} - \frac{1}{T_m} \right) \right] \quad (6.10)$$

$$K_i = K_i^o \exp \left[\frac{-\Delta H_i}{R} \left(\frac{1}{T} - \frac{1}{T_m} \right) \right] \quad (6.11)$$

6.3 Kinetic parameter estimation

These set of nonlinear differential algebraic equations were fitted against the experimental data by using nonlinear regression analysis. A close match between the experimental data and the model prediction is due to higher value of correlation coefficient ($R^2 > 0.99$). In fact, a good fit between the kinetic model and experimental data is revealed by the Figure 6.9.

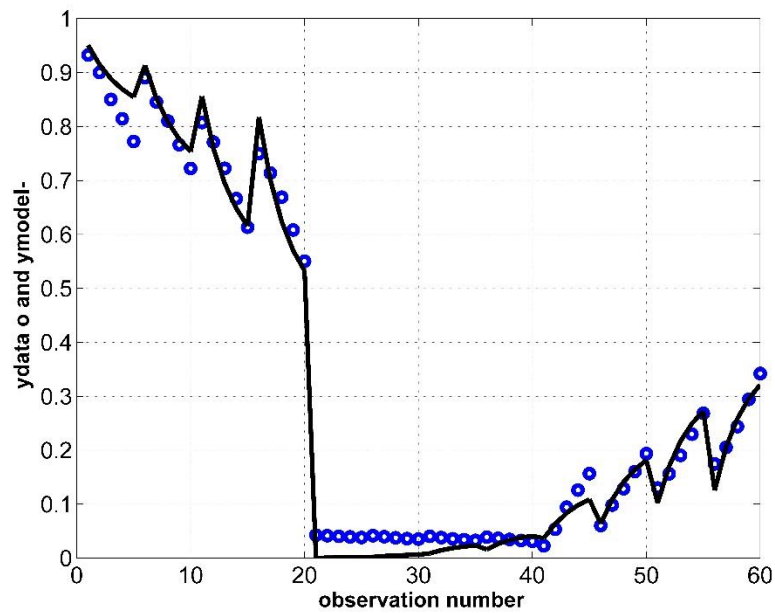


Figure 6.9. Experimental data points and model prediction vs observation number

The experimental points are represented by the blue circles while the continuous black line presents the trend of the model. The close coincidence between the predicted and experimental points, indicates good fitting.

The estimated activation energies and pre-exponential factor values are shown in Table 6.1. The activation energies values for the desired reaction and nonselective reactions are almost identical, that confirm the competitive reaction network for the C4-olefins production. The kinetic model further verified the experimental results for the ODH of butane in gas phase oxygen free condition, in which higher selectivity was observed at low reaction temperature. Actually the ratio of rate of reaction value for the desired reaction to that of CO_x decreases with increase in the temperature. While, higher rate constant for CO_x production was observed at higher temperature.

Table 6.1. Estimated kinetic parameters at 450 °C

Parameters	Units	Values
$k_{C_4H_{10}}$	mol / kg sec	4.0E-06
$k_{C_4H_8}$	mol / kg sec	3.01E-06
k_{CO_x}	mol / kg sec	1.60E-08
$E_{C_4H_{10}}$	kJ / mol	130.31
$E_{C_4H_8}$	kJ / mol	149.89
E_{CO_x}	kJ / mol	135.13
$K_{C_4H_{10}}$	ml / mol	58.13
$K_{C_4H_8}$	ml / mol	65.89
$\Delta H_{C_4H_{10}}$	kJ / mol	-85.17
$\Delta H_{C_4H_8}$	kJ / mol	-31.03
λ	-	0.018

Figures 6.10 and 6.11 shows the model predicted (continuous line) mole fraction and well as experimental data points (circles) for both CO_x and for C4-olefins at 550 °C and 575 °C and for varying residence time. Higher mole fraction of CO_x is due to higher rate of formation of the CO_x compared to olefins production. Secondly, at elevated temperature C4-olefins also tend to give complete combustion products.

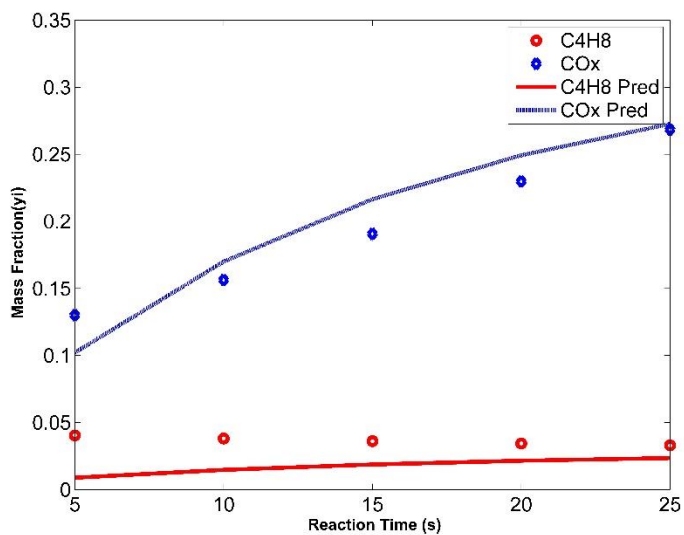


Figure 6.10. Model predicted (continuous line) mole fraction and experimental data points (circles) for both CO_x and for C4-olefins at 550°C

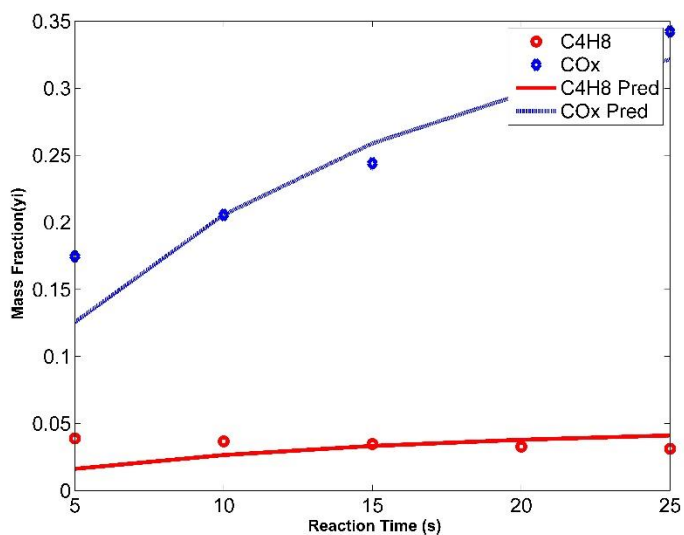


Figure 6.11. Model predicted (continuous line) mole fraction and experimental data points (circles) for both CO_x and for C4-olefins at 550°C

6.4 Comparison with the literature

Recently, Bing Xu et al. reported 30.3% n-butane conversion and total butene selectivity of 64.3% over a 5%-V₂O₅/MgO-Al₂O₃ at 600 °C in a fixed bed quartz tube reactor [63]. X. Wang et al. impregnated different wt% of VO_x on mesoporous MCM-41 support and were able to obtain 47.4% feed conversion and 57% C₄-olefins selectivity in a stainless steel fixed bed reactor operated at 550 °C [33]. In the separate study, vanadium oxide was impregnated on different support materials, e.g. α-Al₂O₃, γ-Al₂O₃, USY, NaY. Among these, VO_x/USY showed highest C₄ olefins selectivity of 68% with 8% n-butane conversion at 520 °C in gas phase O₂ free condition by using a fixed-bed reactor [30]. While E.M. Garcia et al. also reported VO_x/USY catalyst with 75% C₄ olefins selectivity and 8% n-butane conversion at 520 °C in fixed-bed micro-reactor under anaerobic reaction condition [36]. In present study, 0.2 Ce catalyst shows C₄-olefins selectivity of 62% and n-butane conversion of 10.7% at 450 °C under anaerobic fluidized-bed reaction condition. So, the synthesized catalyst in the present study has comparable performance with already reported catalysts in the literature. The higher catalytic activity and good stability of VO_x/Ce-MAs catalysts at low reaction temperature make them very suitable for anaerobic fluidized bed ODH reactions.

CHAPTER 7

CONCLUSIONS AND RECOMMENDATIONS

A fluidizable VO_x based catalysts were prepared by template free synthesis method and then they were first screened based on the different state of art characterization techniques. Later, the catalytic performance was evaluated in novel CREC Riser Simulator for ODH of butane under anaerobic condition. Finally, Langmuir-Henshelwood based kinetic model was fitted by nonlinear regression analysis, giving higher correlation value.

7.1 Conclusions

The XRD, Raman and FTIR analysis confirmed the presence of crystalline CeO₂, while no peak for crystalline V₂O₅ phase were observed. TPR/TPO analysis revealed that VO_x/Ce- MAs catalysts are very stable over the repeated reduction and oxidation. NH₃-TPD characterization showed both weak and strong acidic sites. NH₃ desorption kinetics revealed weak metal support interaction with activation energy for NH₃ desorption decreasing in the following order 0.2 Ce > 1.0 Ce > 3.0 Ce > 5.0 Ce. The maximum C4-olefin selectivity of 62% over the 0.2 Ce catalyst was observed at 450 °C and 5 sec contact time mainly because of its mild acidity and strong metal-support interaction. Secondly, it was found that higher reaction temperature and long contact time favors the formation of non-selective products that are CO_x and cracking fractions. The reduced catalyst was found to be more selective than the freshly prepared catalyst. Overall, the regression analysis has shown a good fitting for the estimation of kinetic parameters. At the low reaction

temperature (450 °C) the kinetic model predicted low activation energy (130.1 kJ mol⁻¹) for the C4-alkenes formation, as compared to high activation energies noticed for the undesired deep oxidation of the feed (135.1 kJ mol⁻¹) and C4-olefins (149.9 kJ mol⁻¹).

7.2 Recommendations

- The combined effect of vanadia and ceria loading on the selectivity of C4-olefin can be studied.
- Different active metal oxides can be impregnated on the promising support.
- As for higher selectivity of C4-olefins basic catalyst is needed, so it is highly recommended to dope this high surface area MAs support with alkali or alkaline earth metals and to evaluate it for ODH of n-butane.
- A higher ceria containing catalysts have more acidity so they can be tested in the cracking reactions.

References

- [1] H.H. Kung, Oxidative Dehydrogenation of Light (C2 to C4) Alkanes, in: *Adv. Catal.* Vol. 40, 1994: pp. 1–38. doi:10.1016/S0360-0564(08)60655-0.
- [2] W.C. White, Butadiene production process overview, *Chem. Biol. Interact.* 166 (2007) 10–14. doi:10.1016/j.cbi.2007.01.009.
- [3] W. Yan, Q.Y. Kouk, J. Luo, Y. Liu, A. Borgna, Catalytic oxidative dehydrogenation of 1-butene to 1,3-butadiene using CO₂, *Catal. Commun.* 46 (2014) 208–212. doi:10.1016/j.catcom.2013.12.016.
- [4] R.K. Grasselli, Fundamental principles of selective heterogeneous oxidation catalysis, *Top. Catal.* 21 (2002) 79–88. doi:10.1023/A:1020556131984.
- [5] M. Bender, An Overview of Industrial Processes for the Production of Olefins - C 4 Hydrocarbons, *ChemBioEng Rev.* 1 (2014) 136–147. doi:10.1002/cben.201400016.
- [6] C.N. Satterfield, *Heterogeneous Catalysis in industrial Practice*, *Heterog. Catal. Pract.* (1980). doi:TP156.C35S27.
- [7] J.J.H.B. Sattler, J. Ruiz-Martinez, E. Santillan-Jimenez, B.M. Weckhuysen, Catalytic Dehydrogenation of Light Alkanes on Metals and Metal Oxides, *Chem. Rev.* 114 (2014) 10613–10653. doi:10.1021/cr5002436.
- [8] S. a. Al-Ghamdi, H.I. de Lasa, Propylene production via propane oxidative dehydrogenation over VO_x/γ-Al₂O₃ catalyst, *Fuel.* 128 (2014) 120–140. doi:10.1016/j.fuel.2014.02.033.

- [9] M.A. Fahim, T.A. Alsahhaf, A. Elkilani, Introduction, in: *Fundam. Pet. Refin.*, Elsevier, 2010: pp. 1–9. doi:10.1016/B978-0-444-52785-1.00001-2.
- [10] C.R. Mistry, R.K. Mewada, V.K. Srivastava, R. V Jasra, Characteristics of Oxidation and Oxidative Dehydrogenation Catalysts for Gas Phase Reactions : A Review, *Int. Conf. Curr. Trends Technol.* (2011) 8–10.
- [11] F. Cavani, N. Ballarini, a. Cericola, Oxidative dehydrogenation of ethane and propane: How far from commercial implementation?, *Catal. Today.* 127 (2007) 113–131. doi:10.1016/j.cattod.2007.05.009.
- [12] F. Cavani, F. Trifirò, Partial oxidation of C2 to C4 paraffins, in: *Basic Princ. Appl. Catal.*, 2004: pp. 19–84. doi:10.1007/978-3-662-05981-4.
- [13] S.W. Weller, A review of: “HETEROGENEOUS CATALYSIS IN PRACTICE,” by Charles N. Satterfield (Massachusetts Institute of Technology), [New York, McGraw-Hill Book Company], 1980. 41 6 pp. [ISBN] 0-07-054875-F., *Chem. Eng. Commun.* 13 (1981) 193–194. doi:10.1080/00986448108928199.
- [14] Journa’, Selective Oxidative Dehydrogenation over V-Mg-O Catalysts, *J. Catal.* 467 (1988) 463–467.
- [15] L.M. Madeira, M.F. Portela, Catalytic oxidative dehydrogenation of n -butane, *Catal. Rev.* 44 (2002) 247–286. doi:10.1081/CR-120001461.
- [16] O. Rubio, J. Herguido, M. Menéndez, Oxidative dehydrogenation of n-butane on V/MgO catalysts-kinetic study in anaerobic conditions, *Chem. Eng. Sci.* 58 (2003) 4619–4627. doi:10.1016/j.ces.2003.07.004.

- [17] D. Bhattacharyya, S.K. Bej, M.S. Rao, Oxidative dehydrogenation of n-butane to butadiene, *Appl. Catal. A Gen.* 87 (1992) 29–43. doi:10.1016/0926-860X(92)80171-8.
- [18] T. Blasco, J.M.L. Nieto, A. Dejoz, M.I. Vazquez, Influence of the Acid-Base Character of Supported Vanadium Catalysts on Their Catalytic Properties for the Oxidative Dehydrogenation of n-Butane, *J. Catal.* 157 (1995) 271–282. doi:10.1006/jcat.1995.1291.
- [19] A. Corma, J.M.L. Nieto, N. Paredes, A. Dejoz, I. Vazquez, Oxidative Dehydrogenation of Propane and N-Butane on V-Mg Based Catalysts, *New Dev. Sel. Oxid. li.* 82 (1994) 113–123. <Go to ISI>://A1994BC20N00011.
- [20] N. Kijima, M. Toba, Y. Yoshimura, A Chemical Potential Diagram and an In-situ X-ray Diffraction Analysis of a V–Mg–O Catalyst Used in the Oxidative Dehydrogenation of n-Butane, *Catal. Letters.* 127 (2008) 63–69. doi:10.1007/s10562-007-9353-9.
- [21] H.H.K. M.A. Char1, D. Patel, M.C. Kung, Selective oxidative dehydrogenation of butane over V-Mg-O catalysts, *J. Catal.* 105 (1987) 483–498. doi:10.1016/0021-9517(87)90076-5.
- [22] D. Patel, P.J. Andersen, Oxidative Dehydrogenation of Butane over Orthovanadates, *J. Catal.* 142 (1990) 132–142.

- [23] O.S. Owen, M.C. Kung, H.H. Kung, The effect of oxide structure and cation reduction potential of vanadates on the selective oxidative dehydrogenation of butane and propane, *Catal. Letters*. 12 (1992) 45–50. doi:10.1007/BF00767187.
- [24] H.H.K. L. Owens, The Effect of Loading of Vanadia on Silica in the Oxidation of Butane, *J. Catal.* 144 (1993) 202–213. doi:10.1006/jcat.1993.1324.
- [25] R.M. Martin-Aranda, M.F. Portela, L.M. Madeira, F. Freire, M. Oliveira, Effect of alkali metal promoters on nickel molybdate catalysts and its relevance to the selective oxidation of butane, *Appl. Catal. A Gen.* 127 (1995) 201–217. doi:10.1016/0926-860X(95)00037-2.
- [26] F.J. Maldonado-Hódar, L.M. Palma Madeira, M. Farinha Portela, The Effects of Coke Deposition on NiMoO₄ Used in the Oxidative Dehydrogenation of Butane, *J. Catal.* 164 (1996) 399–410. doi:10.1006/jcat.1996.0396.
- [27] H. Armendariz, J.A. Toledo, G. Aguilar-Rios, M.A. Valenzuela, P. Salas, A. Cabral, et al., Oxidative dehydrogenation of n-butane on zinc-chromium ferrite catalysts, *J. Mol. Catal.* 92 (1994) 325–332. doi:10.1016/0304-5102(94)00071-9.
- [28] D.L. Stern, J.N. Michaels, L. DeCaul, R.K. Grasselli, Oxydehydrogenation of n-butane over promoted Mg□V-oxide based catalysts, *Appl. Catal. A Gen.* 153 (1997) 21–30. doi:10.1016/S0926-860X(97)80115-9.
- [29] M. Sun, J. Zhang, P. Putaj, V. Caps, F. Lefebvre, J. Pelletier, et al., Catalytic oxidation of light alkanes (C₁-C₄) by heteropoly compounds, *Chem. Rev.* 114 (2014) 981–1019. doi:10.1021/cr300302b.

- [30] M. Volpe, G. Tonetto, H. de Lasa, Butane dehydrogenation on vanadium supported catalysts under oxygen free atmosphere, *Appl. Catal. A Gen.* 272 (2004) 69–78. doi:10.1016/j.apcata.2004.05.017.
- [31] D. Bhattacharyya, S.K. Bej, M.S. Rao, Oxidative dehydrogenation of n-butane to butadiene, *Appl. Catal. A Gen.* 87 (1992) 29–43. doi:10.1016/0926-860X(92)80171-8.
- [32] C. Wan, D. Cheng, F. Chen, X. Zhan, Characterization and kinetic study of BiMoLax oxide catalysts for oxidative dehydrogenation of 1-butene to 1,3-butadiene, *Chem. Eng. Sci.* 135 (2014) 1–6. doi:10.1016/j.ces.2014.08.020.
- [33] X. Wang, G. Zhou, Z. Chen, W. Jiang, H. Zhou, In-situ synthesis and characterization of V-MCM-41 for oxidative dehydrogenation of n-butane, *Microporous Mesoporous Mater.* (2015) 1–7. doi:10.1016/j.micromeso.2015.06.029.
- [34] B. Xu, X. Zhu, Z. Cao, L. Yang, W. Yang, Catalytic oxidative dehydrogenation of n-butane over V₂O₅/MO-Al₂O₃ (M = Mg, Ca, Sr, Ba) catalysts, *Chinese J. Catal.* 36 (2015) 1060–1067. doi:10.1016/S1872-2067(15)60839-7.
- [35] M. Setnička, P. Čičmanec, R. Bulánek, A. Zukal, J. Pastva, Hexagonal mesoporous titanosilicates as support for vanadium oxide - Promising catalysts for the oxidative dehydrogenation of n-butane, *Catal. Today.* 204 (2013) 132–139. doi:10.1016/j.cattod.2012.07.028.

- [36] E.M. Garcia, M.D. Sanchez, G. Tonetto, M.A. Volpe, Preparation of USY zeolite supported catalysts from $V(\text{AcAc})_3$ and NH_4VO_3 . Catalytic properties for the dehydrogenation of n-butane in oxygen-free atmosphere, *J. Colloid Interface Sci.* 292 (2005) 179–185. doi:<http://dx.doi.org/10.1016/j.jcis.2005.05.055>.
- [37] I.E. Wachs, B.M. Weckhuysen, Structure and reactivity of surface vanadium oxide species on oxide supports, *Appl. Catal. A Gen.* 157 (1997) 67–90. doi:[10.1016/S0926-860X\(97\)00021-5](https://doi.org/10.1016/S0926-860X(97)00021-5).
- [38] L. Owens, H.H. Kung, Effect of Cesium Modification of Silica-Supported Vanadium-Oxide Catalysts in Butane Oxidation, *J. Catal.* 148 (1994) 587–594. doi:[10.1006/jcat.1994.1245](https://doi.org/10.1006/jcat.1994.1245).
- [39] A. a. Lemonidou, Oxidative dehydrogenation of C₄ hydrocarbons over VMgO catalyst - Kinetic investigations, *Appl. Catal. A Gen.* 216 (2001) 277–284. doi:[10.1016/S0926-860X\(01\)00566-X](https://doi.org/10.1016/S0926-860X(01)00566-X).
- [40] J. Herguido, M. Mene, J. Santamarı, Oxidative Dehydrogenation of n-Butane in a Two-Zone Fluidized-Bed Reactor, *Ind. Eng. Chem. Res.* 38 (1999) 90–97.
- [41] R. Grabowski, Kinetics of Oxidative Dehydrogenation of C₂-C₃ Alkanes on Oxide Catalysts, *Catal. Rev.* 48 (2006) 199–268. doi:[10.1080/01614940600631413](https://doi.org/10.1080/01614940600631413).
- [42] S.A. Al-Ghamdi, H.I. de Lasa, Propylene production via propane oxidative dehydrogenation over $\text{VO}_x/\gamma\text{-Al}_2\text{O}_3$ catalyst, *Fuel.* 128 (2014) 120–140. doi:[10.1016/j.fuel.2014.02.033](https://doi.org/10.1016/j.fuel.2014.02.033).

- [43] G. Ertl, H. Knözinger, F. Schüth, J.W. Editors, W.V. Gmbh, C. Kga, Second , Completely Revised and Enlarged Edition Volume 2, 2008.
- [44] J. Čejka, Organized mesoporous alumina: synthesis, structure and potential in catalysis, *Appl. Catal. A Gen.* 254 (2003) 327–338. doi:10.1016/S0926-860X(03)00478-2.
- [45] C. Morterra, G. Magnacca, A case study: surface chemistry and surface structure of catalytic aluminas, as studied by vibrational spectroscopy of adsorbed species, *Catal. Today.* 27 (1996) 497–532. doi:10.1016/0920-5861(95)00163-8.
- [46] B. Huang, C.H. Bartholomew, B.F. Woodfield, Facile synthesis of mesoporous γ -alumina with tunable pore size: The effects of water to aluminum molar ratio in hydrolysis of aluminum alkoxides, *Microporous Mesoporous Mater.* 183 (2014) 37–47. doi:10.1016/j.micromeso.2013.09.007.
- [47] W. Cai, J. Yu, M. Jaroniec, Template-free synthesis of hierarchical spindle-like γ -Al₂O₃ materials and their adsorption affinity towards organic and inorganic pollutants in water, *J. Mater. Chem.* 20 (2010) 4587. doi:10.1039/b924366f.
- [48] C. Yang, L. Gao, Y. Wang, X. Tian, S. Komarneni, Fluoride removal by ordered and disordered mesoporous aluminas, *Microporous Mesoporous Mater.* 197 (2014) 156–163. doi:10.1016/j.micromeso.2014.06.010.
- [49] A. Trovarelli, C. de Leitenburg, M. Boaro, G. Dolcetti, The utilization of ceria in industrial catalysis, *Catal. Today.* 50 (1999) 353–367. doi:10.1016/S0920-5861(98)00515-X.

- [50] H. Yao, Ceria in automotive exhaust catalysts I. Oxygen storage, *J. Catal.* 86 (1984) 254–265. doi:10.1016/0021-9517(84)90371-3.
- [51] J. Guzman, S. Carrettin, A. Corma, Spectroscopic Evidence for the Supply of Reactive Oxygen during CO Oxidation Catalyzed by Gold Supported on Nanocrystalline CeO₂, *J. Am. Chem. Soc.* 127 (2005) 3286–3287. doi:10.1021/ja043752s.
- [52] J. Kašpar, P. Fornasiero, M. Graziani, Use of CeO₂-based oxides in the three-way catalysis, *Catal. Today.* 50 (1999) 285–298. doi:10.1016/S0920-5861(98)00510-0.
- [53] Q. Sun, Y. Zheng, Z. Li, Y. Zheng, Y. Xiao, G. Cai, et al., Studies on the improved thermal stability for doped ordered mesoporous γ -alumina., *Phys. Chem. Chem. Phys.* 15 (2013) 5670–6. doi:10.1039/c3cp50190f.
- [54] E. Moretti, M. Lenarda, L. Storaro, A. Talon, R. Frattini, S. Polizzi, et al., Catalytic purification of hydrogen streams by PROX on Cu supported on an organized mesoporous ceria-modified alumina, *Appl. Catal. B Environ.* 72 (2007) 149–156. doi:10.1016/j.apcatb.2006.10.020.
- [55] G. Raju, B.M. Reddy, S.-E. Park, CO₂ promoted oxidative dehydrogenation of n-butane over VO_x/MO₂-ZrO₂ (M=Ce or Ti) catalysts, *J. CO₂ Util.* 5 (2014) 41–46. doi:10.1016/j.jcou.2013.12.003.
- [56] X. Shang, X. Wang, W. Nie, X. Guo, X. Zou, W. Ding, et al., Facile strategy for synthesis of mesoporous crystalline γ -alumina by partially hydrolyzing aluminum nitrate solution, *J. Mater. Chem.* 22 (2012) 23806. doi:10.1039/c2jm35508f.

- [57] J. Wang, K. Shang, Y. Guo, W.-C. Li, Easy hydrothermal synthesis of external mesoporous γ -Al₂O₃ nanorods as excellent supports for Au nanoparticles in CO oxidation, *Microporous Mesoporous Mater.* 181 (2013) 141–145. doi:10.1016/j.micromeso.2013.07.028.
- [58] B.D. Cullity, *Elements of X-Ray Diffraction*, (1956) 514.
- [59] H.I. De Lasa, Canadian Patent 1,284,017,(1991), USA Pat. 5 (1992).
- [60] S. Al-Ghamdi, M. Volpe, M.M. Hossain, H. De Lasa, VO_x/c-Al₂O₃ catalyst for oxidative dehydrogenation of ethane to ethylene: Desorption kinetics and catalytic activity, *Appl. Catal. A Gen.* 450 (2013) 120–130. doi:10.1016/j.apcata.2012.10.007.
- [61] A.H. Elbadawi, M.S. Ba-Shammakh, S. Al-Ghamdi, S.A. Razzak, M.M. Hossain, Reduction kinetics and catalytic activity of VO_x/ γ -Al₂O₃-ZrO₂ for gas phase oxygen free ODH of ethane, *Chem. Eng. J.* 284 (2016) 448–457. doi:10.1016/j.cej.2015.08.048.
- [62] I. a. Bakare, S. a. Mohamed, S. Al-Ghamdi, S. a. Razzak, M.M. Hossain, H.I. de Lasa, Fluidized bed ODH of ethane to ethylene over VO_x-MoO_x/ γ -Al₂O₃ catalyst: Desorption kinetics and catalytic activity, *Chem. Eng. J.* (2014). doi:10.1016/j.cej.2014.09.114.
- [63] B. Xu, X. Zhu, Z. Cao, L. Yang, W. Yang, Catalytic oxidative dehydrogenation of n-butane over V₂O₅/MO-Al₂O₃ (M = Mg, Ca, Sr, Ba) catalysts, *Chinese J. Catal.* 36 (2015) 1060–1067. doi:10.1016/S1872-2067(15)60839-7.

- [64] A. Khodakov, J. Yang, S. Su, E. Iglesia, A.T. Bell, Structure and properties of vanadium oxide-zirconia catalysts for propane oxidative dehydrogenation, *J. Catal.* 177 (1998) 343–351. doi:10.1006/jcat.1998.2143.
- [65] J.P. Bortolozzi, T. Weiss, L.B. Gutierrez, M.A. Ulla, Comparison of Ni and Ni–Ce/Al₂O₃ catalysts in granulated and structured forms: Their possible use in the oxidative dehydrogenation of ethane reaction, *Chem. Eng. J.* 246 (2014) 343–352. doi:10.1016/j.cej.2014.02.078.
- [66] S. Boullouso-Eiras, E. Vanhaecke, T. Zhao, D. Chen, A. Holmen, Raman spectroscopy and X-ray diffraction study of the phase transformation of ZrO₂–Al₂O₃ and CeO₂–Al₂O₃ nanocomposites, *Catal. Today.* 166 (2011) 10–17. doi:10.1016/j.cattod.2010.05.038.
- [67] M.S.P. Francisco, V.R. Mastelaro, P. a P. Nascente, A.O. Florentino, Activity and characterization by XPS, HR-TEM, Raman spectroscopy, and bet surface area of CuO/CeO₂-TiO₂ catalysts, *J. Phys. Chem. B.* 105 (2001) 10515–10522. doi:10.1021/jp0109675.
- [68] M.-E. Becerra, N.-P. Arias, O.-H. Giraldo, F.-E. Lopez-Suarez, M.-J. Illan-Gomez, A. Bueno-Lopez, Alumina-supported manganese catalysts for soot combustion prepared by thermal decomposition of kMnO₄, *Catalysts.* 2 (2012) 352–367. doi:10.3390/catal2030352.

- [69] C. Yu, J. Hu, W. Zhou, Q. Fan, Novel Ni/CeO₂-Al₂O₃ composite catalysts synthesized by one-step citric acid complex and their performance in catalytic partial oxidation of methane, *J. Energy Chem.* 23 (2014) 235–243. doi:10.1016/S2095-4956(14)60141-8.
- [70] Y. Shigesato, M. Enomoto, H. Odaka, Thermo-chromic VO₂ Films Deposited by RF Magnetron Sputtering Using V₂O₃ or V₂O₅ Targets, *Jpn. J. Appl. Phys.* 39 (2000) 6016. doi:10.1143/JJAP.39.6016.
- [71] A. Trovarelli, Catalytic Properties of Ceria, *Catal. Rev.* 38 (2006) 439–520.
- [72] C.H. Bartholomew, *Fundamentals of industrial toxicology*, 1982. doi:10.1016/S0015-6264(82)80243-5.
- [73] R.J. Cvetanovi, Y. Amenomiya, Application of a Temperature-Programmed Desorption Technique to Catalyst Studies, (1996) 1996.
- [74] N. Topsoe, Infrared and temperature-programmed desorption study of the acidic properties of ZSM-5-type zeolites, *J. Catal.* 70 (1981) 41–52. doi:10.1016/0021-9517(81)90315-8.
- [75] Z. Wu, R. Jin, Y. Liu, H. Wang, Ceria modified MnO_x/TiO₂ as a superior catalyst for NO reduction with NH₃ at low-temperature, *Catal. Commun.* 9 (2008) 2217–2220. doi:10.1016/j.catcom.2008.05.001.

- [76] K.J. Lee, P.A. Kumar, M.S. Maqbool, K.N. Rao, K.H. Song, H.P. Ha, Ceria added Sb-V₂O₅/TiO₂ catalysts for low temperature NH₃ SCR: Physico-chemical properties and catalytic activity, *Appl. Catal. B Environ.* 142-143 (2013) 705–717. doi:10.1016/j.apcatb.2013.05.071.
- [77] R.J. Cvetanović, Y. Amenomiya, A Temperature Programmed Desorption Technique for Investigation of Practical Catalysts, *Catal. Rev.* 6 (1972) 21–48. doi:10.1080/01614947208078690.
- [78] G. Tonetto, J. Atias, H. De Lasa, FCC catalysts with different zeolite crystallite sizes: Acidity, structural properties and reactivity, *Appl. Catal. A Gen.* 270 (2004) 9–25. doi:10.1016/j.apcata.2004.03.042.
- [79] K.E. Sedor, M.M. Hossain, H.I. de Lasa, Reactivity and stability of Ni/Al₂O₃ oxygen carrier for chemical-looping combustion (CLC), *Chem. Eng. Sci.* 63 (2008) 2994–3007. doi:10.1016/j.ces.2008.02.021.
- [80] E. Reddy, Preparation, characterization, and activity of Al₂O₃-supported V₂O₅ catalysts, *J. Catal.* 221 (2004) 93–101. doi:10.1016/j.jcat.2003.07.011.
- [81] M. MARTINEZHUERTA, X. GAO, H. TIAN, I. WACHS, J. FIERRO, M. BANARES, Oxidative dehydrogenation of ethane to ethylene over alumina-supported vanadium oxide catalysts: Relationship between molecular structures and chemical reactivity, *Catal. Today.* 118 (2006) 279–287. doi:10.1016/j.cattod.2006.07.034.

- [82] M.M. Koranne, J.G. Goodwin, G. Marcelin, Characterization of Silica- and Alumina-Supported Vanadia Catalysts Using Temperature Programmed Reduction, *J. Catal.* 148 (1994) 369–377. doi:10.1006/jcat.1994.1217.
- [83] R. Sasikala, N. Gupta, S. Kulshreshtha, Temperature-programmed reduction and CO oxidation studies over Ce–Sn mixed oxides, *Catal. Letters.* 71 (2001) 69–73. doi:10.1023/A:1016656408728.
- [84] Y. Nakajima, Y. Endo, Y. Inoue, K. Yamanaka, K. Kato, H. Wanibuchi, et al., Ingestion of Hijiki seaweed and risk of arsenic poisoning, *Appl. Organomet. Chem.* 20 (2006) 557–564. doi:10.1002/aoc.

Vitae

Name	:MUHAMMAD YASIR KHAN
Nationality	:PAKISTANI
Date of Birth	:7/27/1989
Email	:m.yasir.khan434@gmail.com
Address	:King Fahd University of petroleum and Minerals
Academic Background	:B.Sc. Chemical Engineering – U. E. T Peshawar

MUHAMMAD YASIR KHAN is a graduating student of Chemical Engineering Department at King Fahd University of Petroleum and Minerals (KFUPM). His CGPA at KFUPM Chemical Engineering Department is 3.96/4. Previously, he did his B.Sc. Chemical Engineering from University of Engineering and Technology Peshawar, Pakistan (UET Peshawar). In the undergraduate, out of 8 semesters, he secured 6 semester positions and got overall 1st Position in the Department of Chemical Engineering, UET Peshawar. His CGPA in B.Sc. Chemical Engineering is 3.68/4 and based on his outstanding academic performance in his undergraduate studies he was awarded University Gold Medal.

Research Outcomes

Journal Papers (in progress):

1. **M Yasir Khan**, Mohammad M. Hossain, Idris A. Bakare, Shaikh A. Razzak, “Gas phase oxygen free ODH of n-butane to C4-Olefins using ceria modified $\text{VO}_x/\gamma\text{-Al}_2\text{O}_3$ catalyst in CREC Riser Simulator”.
2. **M Yasir Khan**, Mohammad M. Hossain, Sameer Al-Ghamdi, Shaikh A. Razzak, “Oxidative dehydrogenation of ethane to ethylene in gas phase oxygen free condition using $\text{VO}_x/\text{CeO}_2\text{-}\gamma\text{-Al}_2\text{O}_3$ catalyst”.
3. **M Yasir Khan**, Mohammad M. Hossain, Sameer Al-Ghamdi, Shaikh A. Razzak, Kinetic modeling of the ODH of n-butane to corresponding butene in gas phase oxygen free condition.